ADVANCED HEALTHCARE MATERIALS
www.advhealthmat.de

Zinc-Based Tannin-Modified Composite Microparticulate Scaffolds with Balanced Antimicrobial Activity and Osteogenesis for Infected Bone Defect Repair

Yitao Zhao, Jintao Li, Lingli Liu, Yue Wang, Yan Ju, Chun Zeng, Zhihui Lu,* Denghui Xie,* and Jinshan Guo**

Treatment of infected bone defects is a major clinical challenge; bioactive materials combining sufficient antimicrobial activity and favorable osteogenic ability are urgently needed. In this study, through a facile one-pot hydrothermal reaction of zinc acetate in the presence of tannic acid (TA), with or without silver nitrate ($AgNO_3$), is used to synthesize a TA or TA and silver nanoparticles (Ag NPs) bulk-modified zinc oxide (ZnO) (ZnO-TA or ZnO-TA-Ag), which is further composited with zein to fabricate porous microparticulate scaffolds for infected bone defect repair. Bulk TA modification significantly improves the release rate of antibacterial metal ions (Zn^{2+} release rate is >100 times that of ZnO). Fast and long-lasting (>35 d) Zn^{2+} and Ag^{+} release guaranteed sufficient antibacterial capability and excellent osteogenic properties in promoting the osteogenic differentiation of bone marrow mesenchymal stem cells and endogenous citric acid production and mineralization and providing considerable immunomodulatory activity in promoting M2 polarization of macrophages. At the same time, synchronously-released TA could scavenge endogenous reactive oxygen species (ROS) and ROS produced by antibacterial metal ions, effectively balancing antibacterial activity and osteogenesis to sufficiently control infection while protecting the surrounding tissue from damage, thus effectively promoting infected bone defect repair.

1. Introduction

The infection rate after internal fixation for bone fractures is 5%–20%, with that for open fractures as high as 30%.[1] Once a post-operative infection occurs, a secondary operation is often required to remove the implant, which may prolong hospitalization and exacerbate the patient's pain.[2] Bone defects caused by high-energy injury are often accompanied by bacterial contamination. Severe bone infections can lead to osteomyelitis and osteonecrosis.[1b,2] Current clinical treatment for bone infections involves the removal of necrotic bone tissue and systemic administration of antibiotics or implantation of antibiotic-laden bone cement (Masquelet technology) for local delivery of antibiotics.[3] However, owing to the difficulty of infection control and repeated infections, these treatments may take months or even years, leading to the postponement of bone regeneration (often after complete removal of the infection source) and even fracture nonunion.[1a,2b] Nondegradable bone cement also needs to be removed prior to the implantation of bone grafts,[4] and long-term exposure to low-dose antibiotics increases the risk of bacterial resistance. Although researchers had developed hydrogels loaded with both lysostaphin and bone morphogenetic protein-2 (BMP-2) to combat bone infection and promote bone regeneration at the same time,[1a,5] the poor stability of lysostaphin greatly limited its practical applications. The development of novel orthopedic biomaterials with sufficient antimicrobial activity and favorable orthopedic ability is urgently needed.

Recently, to address bone infection problems, silver nanoparticles (Ag NPs) have been introduced onto the surfaces of hydroxyapatite (HA)[2b,6] or medical titanium alloys.[7] Copper-substituted HA,[8] red phosphorous-metal composites, magnesium-modified black phosphorus,[9] zinc (Zn)-copper alloys,[10] and magnesium/Zn metal organic frameworks (MOFs)[11] with antimicrobial properties have also been developed. Among aforementioned antimicrobial metal or inorganic ions, Zn had attracted intensive research attention,[10,11] owing to the favorable osteogenic ability of Zn. As an important trace metal element, ≈29% of Zn in the human body is located in the skeletal system[12] and can promote the proliferation of osteoblasts and expression of alkaline phosphatase (ALP) and Runt-related transcription factor 2 (Runx2) from osteoblasts.[13]

Y. Zhao, J. Li, L. Liu, Y. Wang, Y. Ju, C. Zeng, Z. Lu, D. Xie, J. Guo
Department of Histology and Embryology
School of Basic Medical Sciences
Department of Orthopedic Surgery
Guangdong Provincial Key Laboratory of Bone and Joint Degeneration Diseases
The Third Affiliated Hospital of Southern Medical University
Southern Medical University
Guangzhou 510515, P. R. China
E-mail: zengdavid@126.com; sanlumo12@smu.edu.cn; xiedenghui221122@smu.edu.cn; jsguo4127@smu.edu.cn

The ORCID identification number(s) for the author(s) of this article can be found under https://doi.org/10.1002/adhm.202300303

DOI: 10.1002/adhm.202300303

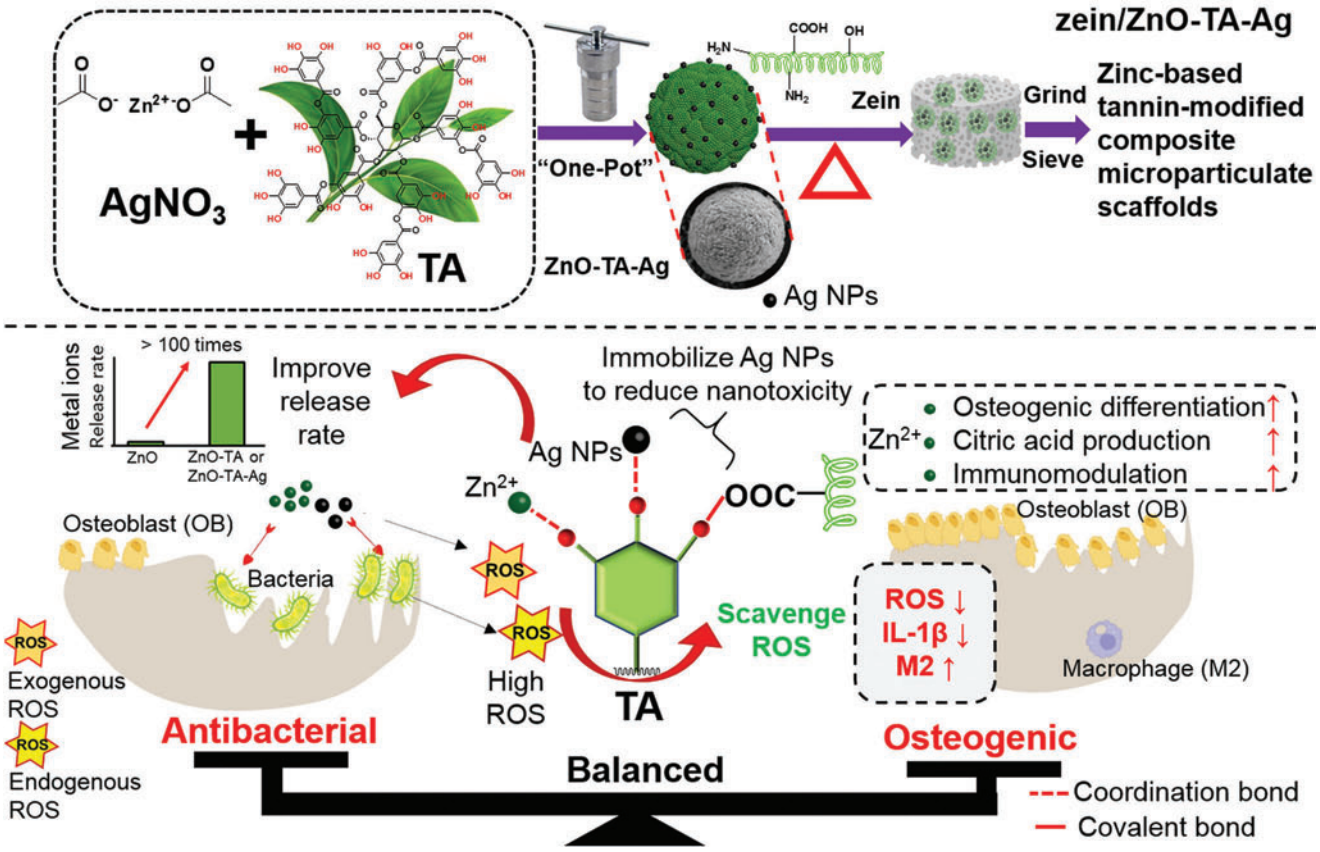

Scheme 1. A) Synthesis of tannic acid (TA) or TA and silver nanoparticles (Ag NPs) bulk-modified zinc oxide (ZnO) (ZnO-TA or ZnO-TA-Ag), and the fabrication of zinc-based tannin-modified composite microparticulate (MP) scaffolds (zein/ZnO-TA and zein/ZnO-TA-Ag); B) ZTCM scaffolds possessed balanced antibacterial activity and osteogenesis, beneficial for infected bone defect repair.

Moreover, clinical studies on the blood serum of more than 3000 patients found that plasma Zn concentration was positively correlated with bone mineral density (BMD).[14] Degenerative orthopedic diseases such as osteoporosis have also been proven to be closely related to the decrease of Zn concentration with aging.[15] The secretion and enrichment of citric acid (CA) by osteoblasts is an indispensable stage in osteogenic differentiation and mineralization of bone marrow mesenchymal stem cells (BMSCs), and osteoblasts are specialized as CA-secreting cells.[16] Zn^{2+} can increase the extracellular accumulation of CA by regulating the tricarboxylic acid (TCA) cycle by controlling the activity of aconitase (ACO_2) and inhibiting the isomerization of CA into isocitric acid and the subsequent oxidization,[15,17] and can promote osteogenic differentiation and mineralization. Furthermore, Zn^{2+} exhibits favorable immunomodulatory functions and can effectively induce the polarization of macrophages (M0) toward the anti-inflammatory M2 phenotype.[18] These advantages greatly support the inclusion of Zn^{2+} in orthopedic biomaterial designs for repairing infected bone defect.

Although promising, traditional Zn-based materials, such as Zn-based salts, cannot effectively regulate the release rate of Zn^{2+}, resulting in a burst release and dose-independent cytotoxicity.[13] In contrast, the release of Zn^{2+} from zinc oxide (ZnO) is too slow to reach an effective level; the reactive oxygen species (ROS) generated by ZnO or other antimicrobial agents used to kill bacteria cause damage to the surrounding tissues.[19] Researchers have reported the use of polydopamine to immobilize in situ reduced Ag nanoparticles (NPs) to reduce the nanotoxicity of Ag NPs.[7] In our previous study, the surface of HA was modified by tannic acid (TA) and in situ reduced silver nitrate ($AgNO_3$) into surface-anchored Ag NPs[6] to provide sufficient antibacterial ability and reduce the burst release of Ag NPs. Polyphenols also possess favorable anti-oxidant capabilities to scavenge ROS.[20]

Herein, through a facile one-pot hydrothermal reaction of zinc acetate in the presence of TA with or without $AgNO_3$, TA or TA and Ag NPs bulk-modified ZnO (ZnO-TA or ZnO-TA-Ag) was synthesized and further composited with zein via thermal crosslinking to fabricate porous Zn-based tannin-modified composite microparticulate (MP) scaffolds (zein/ZnO-TA or zein/ZnO-TA-Ag) for infected bone defect repair (**Scheme 1**A). The introduction of Zn^{2+}-TA coordination bonds conferred ZnO-TA and ZnO-TA-Ag with a tremendously improved Zn^{2+} release rate (>100 times that of pure ZnO), and the concurrently released TA can scavenge endogenous ROS and ROS produced by antibacterial Zn^{2+} and Ag^{+}. The zein composition further immobilized the in situ anchored Ag NPs by forming chemical crosslinking between the pyrogallol groups of TA and zein, which

is beneficial for the further reduction of the nanotoxicity of Ag NPs. The antimicrobial, anti-oxidant and anti-inflammatory, immunomodulatory, and osteogenic properties of ZnO-TA, ZnO-TA-Ag, zein/ZnO-TA, and zein/ZnO-TA-Ag composite scaffolds were thoroughly investigated both in vitro and in vivo. The polyphenol bulk modification route of ZnO serves as a versatile platform that not only significantly accelerating the release of antimicrobial metal ions (Zn^{2+} and Ag^{+}) but also balancing the antimicrobial activity and osteogenic properties by providing strong anti-oxidant activity through polyphenols to promote infected bone repair.

2. Results and Discussion

2.1. Cytotoxicity of Zn^{2+} and Its Effect on the Endogenous Production of Citrate by Osteogenic Differentiated rBMSCs

The cytotoxicity of Zn^{2+} against rat bone marrow mesenchymal stem cells (rBMSCs) was assessed by cell counting kit 8 (CCK-8). As shown in Figure S1A, Supporting Information, it can be seen that there was nearly no cytotoxicity against rBMSCs when the concentration of Zn^{2+} was <200 μM, and Zn^{2+} at ≈5–40 μM could promote rBMSCs' proliferation (Figure S1B, Supporting Information).

When rBMSCs were treated with Zn^{2+} during osteogenic differentiation, it is found that Zn^{2+} at ≈5–40 μM (especially ≈20–40 μM) promoted the endogenous citrate production of the osteogenic differentiated rBMSCs (Figure S1C, Supporting Information), agreeing with the reported theory that Zn^{2+} can regulate TCA cycle of osteoblast thus promote the endogenous citrate production.[17] Furthermore, the effect of Zn^{2+} on the energy production of the osteogenic differentiated rBMSCs was also studied by adenosine triphosphate (ATP) kit. Figure S1D, Supporting Information, reveals that the ATP production of the osteogenic differentiated rBMSCs was not affected by the inclusion of Zn^{2+} (Figure S1D, Supporting Information). These results show that certain amount of Zn^{2+} can promote the secretion of endogenous citrate from osteoblast, with the intracellular ATP content almost unaffected, which may be regulated by the powerful intracellular energy metabolic compensation. To our knowledge, this is the first experimental evidence that the inclusion of Zn^{2+} in the osteogenic differentiation of MSCs could promote the endogenous citrate production, and the effective concentration window of Zn^{2+} was also given here.

2.2. Synthesis and Characterizations of ZnO-TA and ZnO-TA-Ag

The synthesis of ZnO-TA and ZnO-TA-Ag adapted from the facile one-pot hydrothermal reaction of ZnO.[21] The successful inclusion of TA in ZnO-TA and ZnO-TA-Ag is confirmed by the show up of the characteristic peaks of TA at ≈1730 cm^{-1} in the FTIR spectra of ZnO-TA and ZnO-TA-Ag, which is assigned to the ester groups of TA (**Figure 1**A). As shown in Figure 1B, the XRD curves of ZnO-TA and ZnO-TA-Ag show the same peaks as ZnO, indicating that TA bulk modification did not change the crystalline structure of ZnO. The show up of the characteristic peaks of Ag NPs in the XRD curve of ZnO-TA-Ag proved the successful introduction of Ag NPs in ZnO-TA-Ag (Figure 1B). Comparing with thermal-stable ZnO which showed only <5 wt% weight loss between 25 and 1000 °C under N_2 atmosphere, ZnO-TA and ZnO-TA-Ag all showed a weight loss of ≈45 wt%, further confirmed the successful introduction of TA and indicated that TA modification was not simply surface modification but bulk modification (Figure 1C). In another words, TA molecules should participate in the internal structure formation of ZnO-TA and ZnO-TA-Ag. Although the existence of Zn^{2+}-TA coordination bonds in ZnO-TA and ZnO-TA-Ag did not change the inside crystalline structure of ZnO, it significantly changed the connection mode between ZnO crystals. This can be clearly reflected by the morphology change of ZnO-TA and ZnO-TA-Ag comparing with that of pure ZnO (Figure 1D–F and Figure S2, Supporting Information): although the sizes of ZnO-TA were similar with that of pure ZnO (10–30 nm), a small but stacked cauliflower morphology was found in ZnO-TA, and ZnO-TA-Ag particles even changed into macro-sized (≈3 μm) spherical morphology. In the case of ZnO-TA-Ag, Ag^{+} was in situ reduced into Ag NPs and one single Ag NP could connect with multiple pyrogallol groups and serve as a crosslinker of ZnO-TA aggregates, leading to a higher level aggregation, thus significantly increased the particle size. The element mapping images of ZnO-TA-Ag shown in Figure 1G as well as the quantitative results in Figure 1H further confirmed the successful introduction of TA (and Ag NPs) in ZnO-TA and ZnO-TA-Ag and proved the uniform distribution of TA and Ag NPs in ZnO-TA-Ag. The element percentages of C in ZnO-TA and ZnO-TA-Ag were calculated to be 9.95 and 8.57 wt%, respectively (Figure 1H), agreeing well with the similar weight losses of them during TGA tests (Figure 1C).

The release of Zn^{2+} and Ag^{+} ions from ZnO-TA and ZnO-TA-Ag particles was measured by ICP-MS. As shown in **Figure 2**A, after the introduction of TA, the cumulative release concentration of Zn^{2+} tremendously increased from <500 ppb (parts per billion) on the 35th day to 6000–8000 ppb for ZnO-TA and ZnO-TA-Ag, respectively on the 35th day, increased ≈100 times. The cumulative release concentration of Ag^{+} from ZnO-TA-Ag reached ≈1 60 000 ppb on the 35th day (Figure 2B). The fast release of Ag^{+} could create a strong antimicrobial crush and the relatively slower but durable Zn^{2+} release ensured the long-term effective antimicrobial performance when treat infected bone defects.

After compositing with zein, the obtained composites were casted into nonporous disks and thermal-crosslinked. The photos of different composite disks are shown in Figure 2C, with zein/HA as control. The degradation profiles of these composite disks were studied. Overall, the degradation rates of the composites in PBS (pH 7.4) were relatively slow, with a mass loss of ≈10 wt% after 5 months, and there was nearly no significant differences between different composites (Figure 2D). In addition, the pH change of the buffer solution collected during composites degradation was also monitored (Figure 2E). During the first 2 weeks, the pH of zein/HA decreased, then stabilized at a pH of 7.2–7.3, while the pH values of the Zein/ZnO, zein/ZnO-TA, and zein/ZnO-TA-Ag groups all stabilized at a pH of 7.4–7.7, indicating that the composites of ZnO and modified ZnO should be biocompatible when implanted in the body (Figure 2E). The in vitro biomineralization results shown in Figure 2F indicate the similar biomineralization ability of the composite disks of ZnO and modified ZnO, and proved that the inclusion of TA did not affect the biomineralization ability.

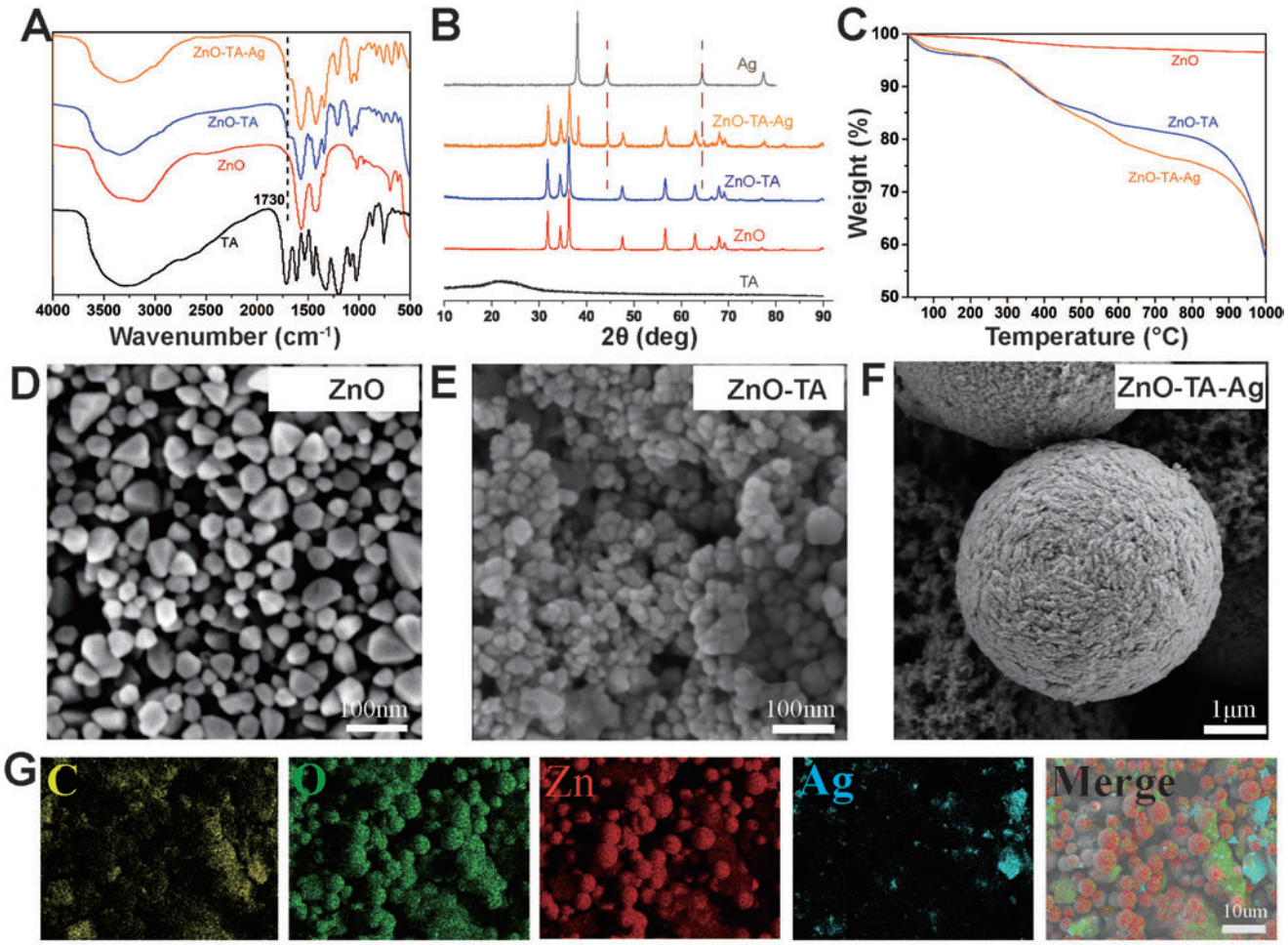

H

Sample	Sample (wt%)			
	C	O	Zn	Ag
ZnO	0	20.72	79.28	0
ZnO-TA	9.95	22.09	67.96	0
ZnO-TA-Ag	8.57	20.53	63.53	7.37

Figure 1. Characterization of TA (± Ag NPs) modified ZnOs: A) FTIR spectra, B) XRD patterns, and C) TGA curves of ZnO, ZnO-TA, ZnO-TA-Ag, and corresponding controls; D–F) SEM images of D) ZnO, E) ZnO-TA, and F) ZnO-TA-Ag; G) element mapping of ZnO-TA-Ag and H) the table of calculated element contents.

2.3. In Vitro Anti-Oxidant Activity of ZnO-TA and ZnO-TA-Ag

The antibacterial ability of ZnO mainly depended on the produced ROS,[19] and excessive ROS generation would bring side effects and impede bone regeneration. As a representative anti-oxidant with plenty phenolic groups, TA was reported possess superior anti-oxidant ability.[20b] Thus the anti-oxidant ability of ZnO-TA and ZnO-TA-Ag was thoroughly investigated via 2,2-diphenyl-1-picrylhydrazyl (DPPH) assay and intracellular ROS assay. As shown in **Figure 3**A,B, the absorption intensity of

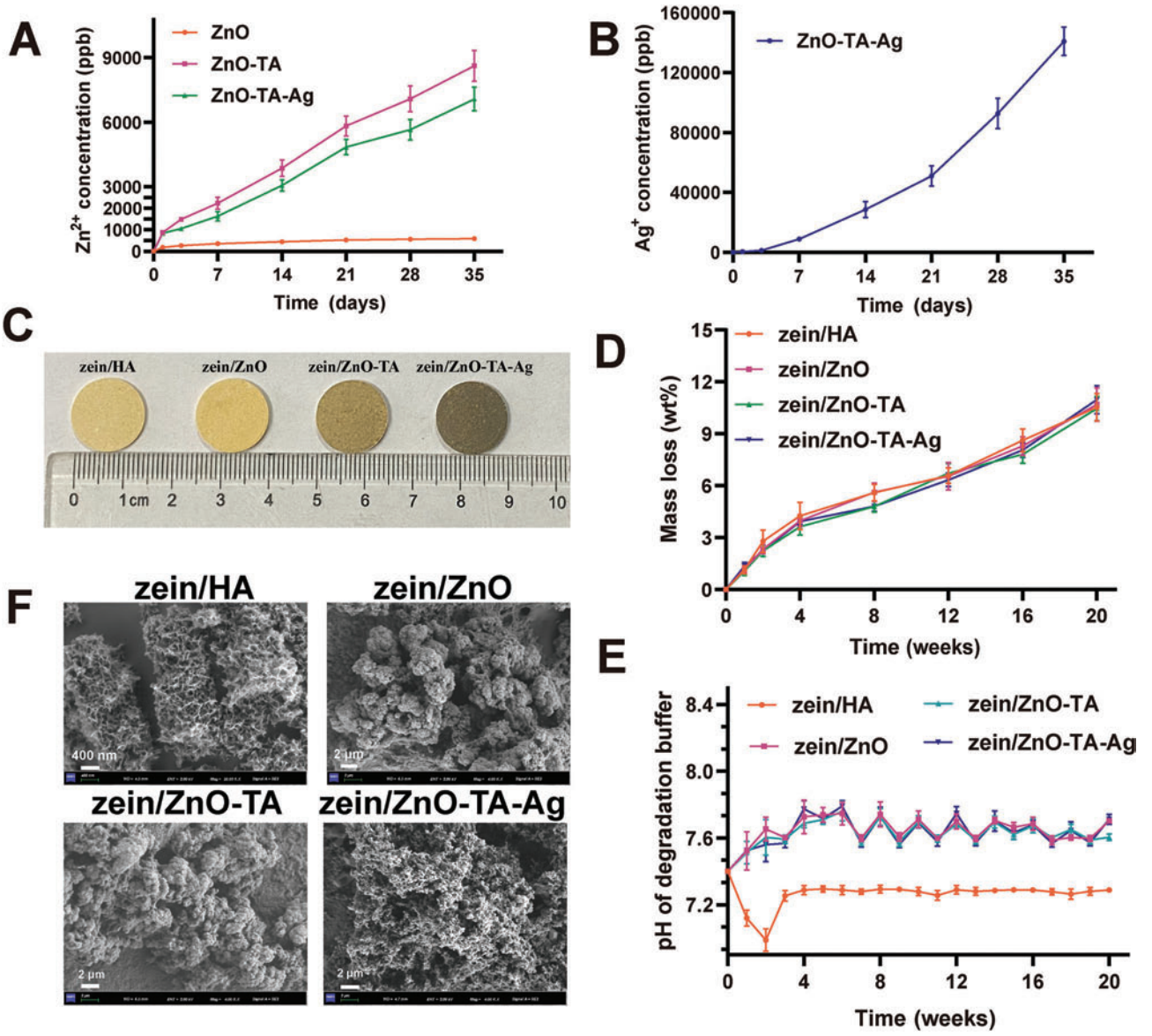

Figure 2. Metal ion release profiles of modified ZnOs and characterizations of their composites with zein: the release profiles of A) Zn^{2+} or B) Ag^{+} from ZnO, ZnO-TA, and ZnO-TA-Ag ($n = 4$); C) representative pictures of zein/HA, zein/ZnO, zein/ZnO-TA, and zein/ZnO-TA-Ag composite disks; change of D) mass losses and E) medium pH values of different composites during in vitro degradation in PBS (pH 7.4) ($n = 5$); F) SEM images of biomineralization deposition on the surface of different composite disks.

DPPH for the ZnO group at 517 nm was close to the blank group, with a DPPH scavenge of only ≈3%. While, the DPPH absorption intensities of the ZnO-TA and ZnO-TA-Ag groups significantly decreased to ≈62% and 66% after 10 min. Further increase of treating time to 20 min resulted in ≈80% DPPH scavenge for ZnO-TA-Ag (Figure 3C). The intracellular ROS level of the HA group was nearly the same as the blank control group, and ZnO induced more ROS as that of ROS UP group, while the inclusion of ZnO-TA and ZnO-TA-Ag significantly reduced the intracellular ROS levels (Figure 3D), which can be also confirmed by the quantitative fluorescent intensity results shown in Figure 3E. These results confirmed the favorable ROS scavenging efficacy of TA modified ZnOs, which could not only reduce the amount of endogenous ROS, but also can effectively reduce the ROS generated by ZnO and Ag NPs, beneficial in providing a good microenvironment for bone regeneration.

2.4. Cytocompatibility and Osteogenic Properties of Zein/ZnO-TA and Zein/ZnO-TA-Ag

The cytocompatibility of ZnO-TA, ZnO-TA-Ag, and their composites with zein was assessed using cytotoxicity tests of modified ZnO and the degradation products of the composites against rBMSCs, with ZnO and the degradation products of the commercially available biocompatible polymer polylactic-*co*-glycolic acid

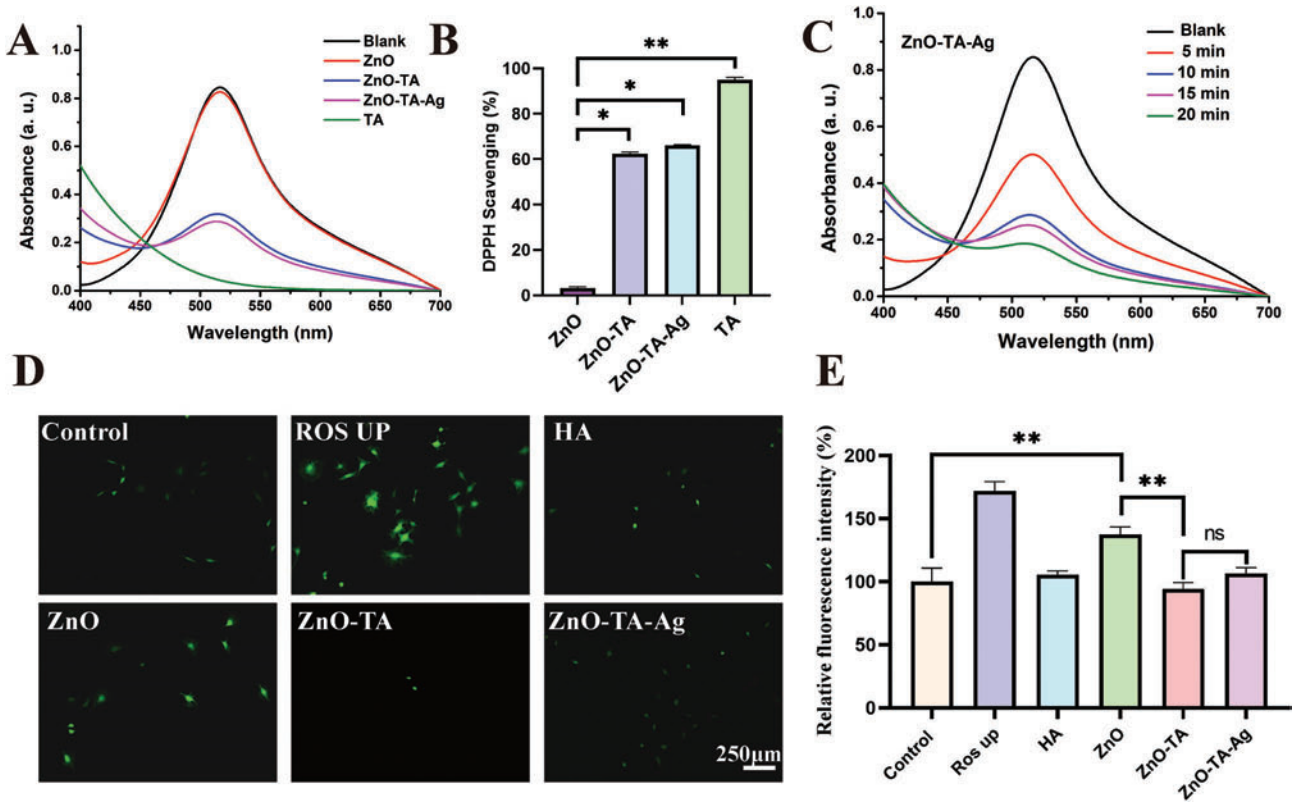

Figure 3. Anti-oxidant activity of modified ZnOs: A) UV–vis spectra and B) DPPH scavenging percentages after incubating for 15 min ($n = 3$); C) the change of UV–vis spectra after the DPPH solution being treated with ZnO-TA-Ag for different times; D) the fluorescence images and E) relative fluorescence intensities of oxidation inhibition obtained by ROS test kit on rBMSCs ($n = 3$). $^{**}p < 0.01$, "ns" represents no significant difference.

(PLGA) as the respective controls. Figure S3A, Supporting Information, shows that there was no significant toxicity for all groups when the concentration of ZnO, ZnO-TA, and ZnO-TA-Ag was <20 μg mL^{-1}, whereas ZnO at concentrations >20 μg mL^{-1} induced significant toxicity, with the cell viabilities <75%. However, the cell viabilities of the ZnO-TA and ZnO-TA-Ag groups were still higher than 75% with concentrations of up to 200 μg mL^{-1}, suggesting that the inclusion of TA not only reduced the toxicity of ZnO but also promoted the proliferation of rBMSCs by accelerating the release of Zn^{2+} (Figure 2A). The favorable anti-oxidant ability of TA (Figure 3A) may explain why ZnO-TA and ZnO-TA-Ag showed much better cytocompatibility than pure ZnO.

Although the cell viabilities of the 1× degradation products of the zein/ZnO, zein/ZnO-TA, and zein/ZnO-TA-Ag composites were lower than 25%, the viabilities were comparable to that of PLGA at 1× dilution (Figure S3B, Supporting Information). The cell viability of the composites significantly increased at 10× and 100× dilutions, particularly at 100× dilution (cell viabilities >95%) (Figure S3B, Supporting Information). The cell proliferation analysis results of the 100× diluted degradation products further confirmed the indicated degradation products of the composites, as shown in the Live/Dead staining images in Figure S3C, Supporting Information, confirming the favorable cytocompatibility of zein/ZnO-TA and zein/ZnO-TA-Ag and supporting their potential in vivo applications.

The osteogenic properties of Zn^{2+}, zein/ZnO-TA, and zein/ZnO-TA-Ag composites were assessed by studying their effects on the osteogenic differentiation of rBMSCs. As shown in **Figure 4**A, the inclusion of 5–40 μmol L^{-1} Zn^{2+} in the osteogenic medium significantly increased the expression levels of ALP, especially on the 14th day, with 10 μmol L^{-1} Zn^{2+} inducing the highest ALP expression level on the 14th day (Figure 4B). As shown in the alizarin red staining images (Figure 4C) and the quantitative red areas on the 14th day (Figure 4D), the inclusion of Zn^{2+} significantly enhanced the mineralization of osteogenic differentiated rBMSCs, especially on the 14th day. After treatment with 100× diluted degradation products of different composite samples in osteogenic medium for 7 days, the expression levels of ALP and Runx2 in the osteogenic differentiated rBMSCs were further studied by Western blotting (WB). The WB strips (Figure 4E) and the corresponding relative protein expression levels (Figure 4F) showed that all the composites of ZnO, ZnO-TA, and ZnO-TA-Ag significantly promoted the expression of ALP and Runx2 (with the zein/ZnO-TA-Ag group showing the highest expression), further confirming the osteogenic efficacy of Zn-based biomaterials.

2.5. The Immunomodulatory Activity of Zein/ZnO-TA and Zein/ZnO-TA-Ag

The immunomodulatory activity of zein/Zno-TA and zein/ZnO-TA-Ag was studied using RAW264.7 as the macrophage cell model (**Figure 5**A). The cytocompatibility of ZnO, ZnO-TA, and

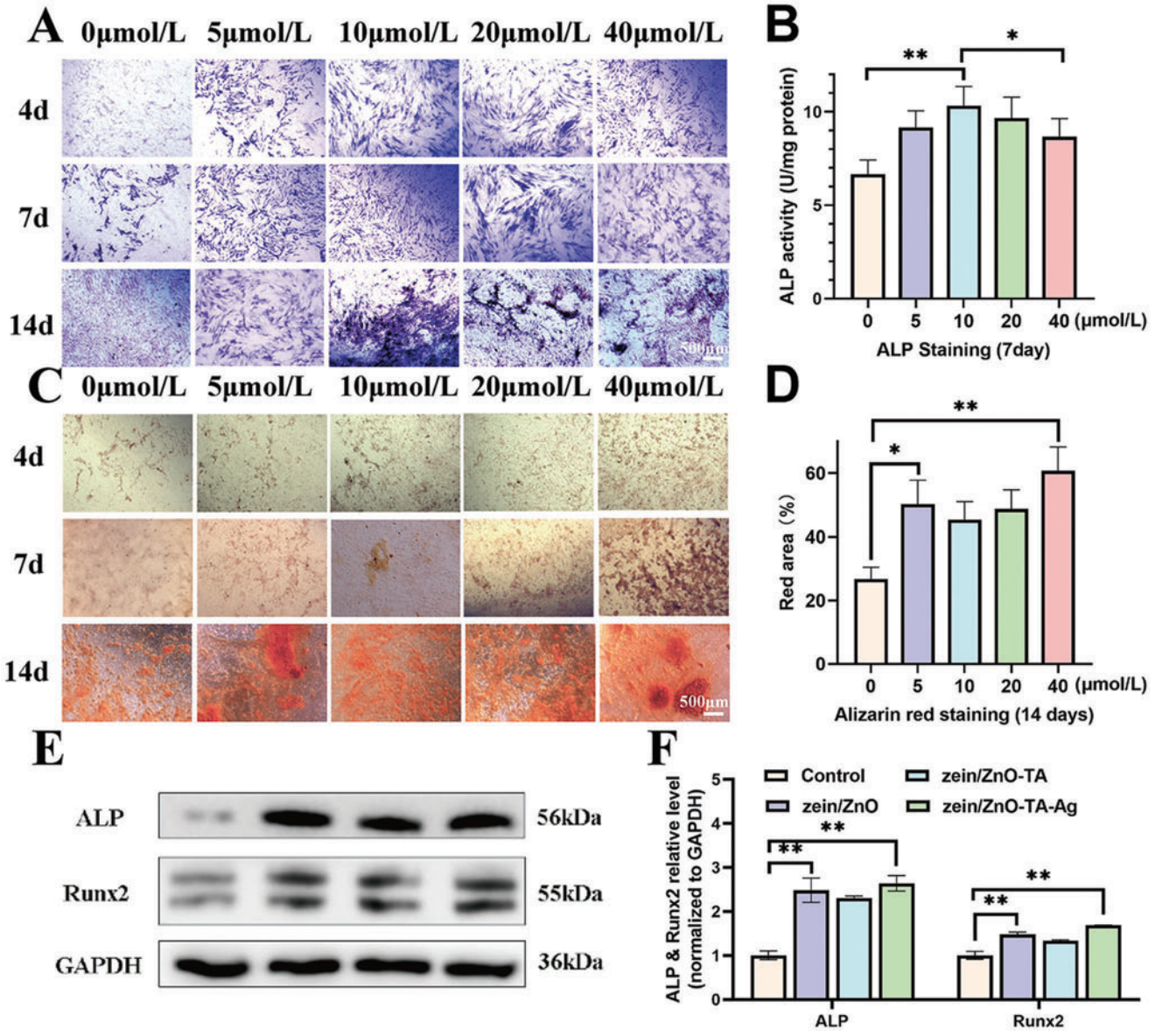

Figure 4. The osteogenic differentiation promotion activity of Zn^{2+} and the composites of modified ZnOs: A) alkaline phosphatase (ALP) staining images and B) quantitative ALP activity (at day 14), C) alizarin red staining images and D) corresponding quantitative red areas at day 14 of BMSCs after being treated with Zn^{2+} with different concentrations in osteogenic media for 4, 7, and 14 days ($n = 3$); E) the Western blotting stripes and F) quantitative protein expression levels of ALP and Runt-related transcription factor 2 (Runx2) after BMSCs being treated with 100× degradation products of different composites in osteogenic media. *$p < 0.05$, **$p < 0.01$.

ZnO-TA-Ag against RAW264.7 was assessed via CCK-8 assay. As shown in Figure 5B, ZnO at concentrations <20 μg mL^{-1} induced less cytotoxicity against RAW264.7, but the toxicity and side effect of ZnO increased with increasing ZnO concentrations, consistent with the cytocompatibility result of rBMSCs. However, with the assistance of anti-oxidant TA, ZnO-TA, and ZnO-TA-Ag caused much less toxicity against RAW264.7, with cell viabilities >90% at a concentration of 100 μg mL^{-1}, significantly higher ($p < 0.05$) than that of ZnO at the same concentration (<60%) (Figure 5B). When the concentration reached 400 μg mL^{-1}, the cell viability of the ZnO group was <30%, whereas those of the ZnO-TA and ZnO-TA-Ag groups were still >60% (Figure 5B), confirming the toxicity reducing effect of including TA into the modified ZnOs.

The effect of different composites on the expression of cell surface markers CD86 and CD206 in RAW264.7 was analyzed using flow cytometry to determine the percentages of cells with M1 or M2 phenotypes. As shown in Figure 5C, the percentage of CD86 positive cells decreased from 45.7% in the LPS (control) group to ≈40% in the zein/ZnO, zein/ZnO-TA, and zein/ZnO-TA-Ag groups. The percentage of the M2 phenotype with positive CD206 marker increased from 0.77% in the LPS group to 6.54%, 12.4%, and 9.01% in the zein/ZnO, zein/ZnO-TA, and zein/ZnO-TA-Ag groups, respectively (Figure 5C). These results

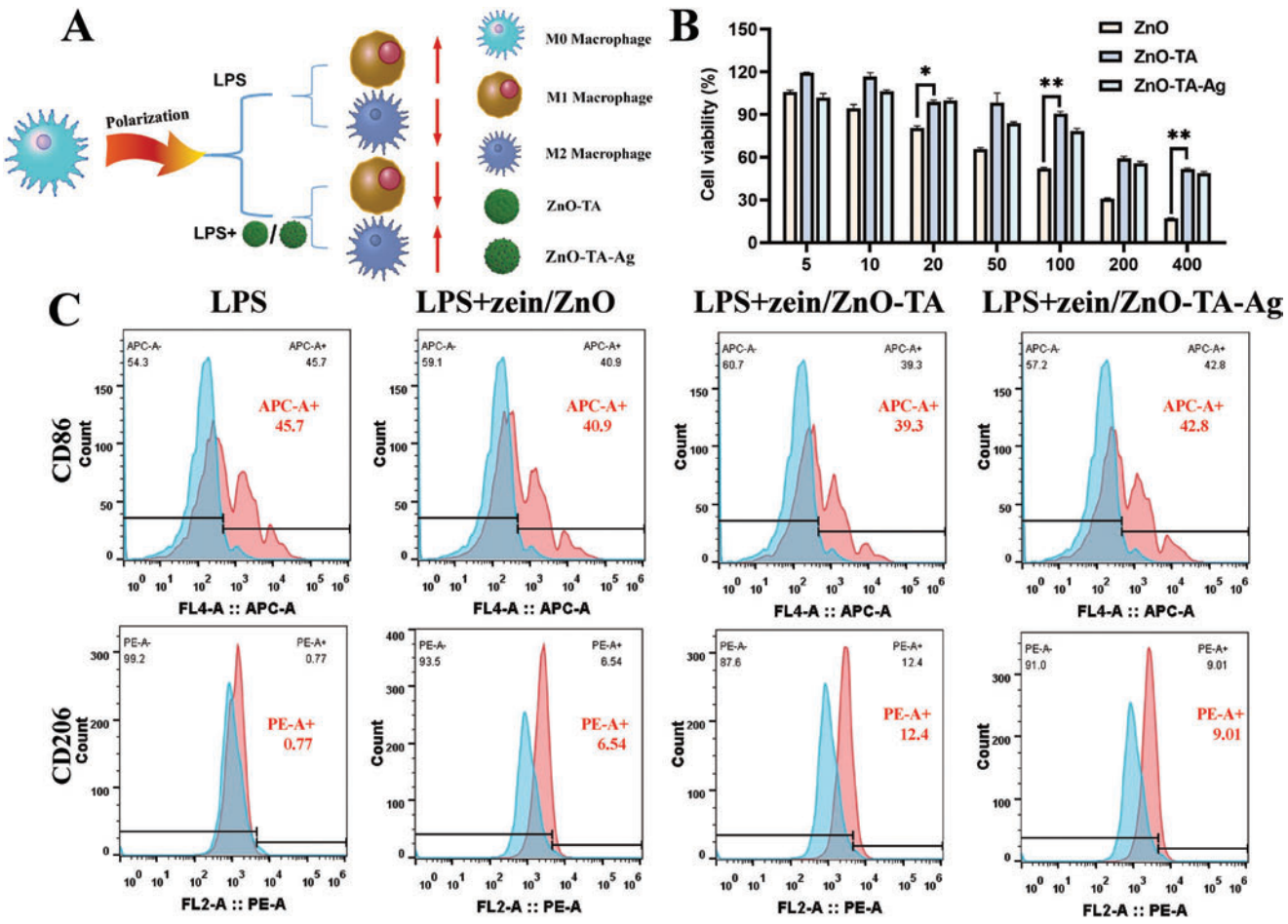

Figure 5. The immunomodulatory activity of modified ZnOs and their composites: A) Schematic illustration of the experiment to study the effect of different composites to the polarization of M0 macrophages; B) cytotoxicity study results of modified ZnOs with different concentrations against RAW264.7; C) representative dot images of surface markers (CD86 and CD206) of RAW264.7 analyzed by flow cytometry. $*p < 0.05$, $**p < 0.01$.

indicate that Zn-based biomaterials promoted the polarization of RAW264.7 from M0 to M2 phenotype but suppressed the polarization of RAW264.7 from M0 to M1 phenotype, agreeing with the results reported in previous literatures.[18] More importantly, the percentages of RAW264.7 in M2 phenotype for the zein/ZnO-TA and zein/ZnO-TA-Ag groups were ≈2.0 or ≈1.5 times higher, respectively, than that of zein/ZnO (Figure 5C), implying that the inclusion of TA in the modified ZnO could further enhance the immunomodulatory activity of ZnO. This may be caused by the tremendously improved Zn^{2+} release rates of ZnO-TA and ZnO-TA-Ag compared to the relatively stable rates of ZnO (Figure 2A,B). The strong anti-oxidant activity provided by TA may also play an important role in the promotion of the immunomodulatory activity of ZnO-TA and ZnO-TA-Ag, which is reflected by the fact that although the inclusion of Ag NPs could produce more ROS, zein/ZnO-TA-Ag still induced more M2 polarization of RAW264.7 than that of zein/ZnO (Figure 5C). The enhanced immunomodulatory activity of the ZnO-TA and ZnO-TA-Ag composites is beneficial for orthopedic applications because the M2 polarized macrophages can promote bone regeneration.

2.6. Antibacterial Performance of ZnO-TA, ZnO-TA-Ag, and Their Composites

The minimum inhibitory concentrations (MICs) of the ZnO, ZnO-TA, and ZnO-TA-Ag particles were assessed using the agar macrodilution method[22] with *Staphylococcus aureus* (*S. aureus*) and *Escherichia coli* (*E. coli*) as representative Gram-positive and Gram-negative bacteria, respectively, with hydroxyapatite (HA) as the control. As shown in **Figure 6**A,B, and Figure S4, Supporting Information, within all the tested concentrations, HA showed almost no antibacterial activity against either *S. aureus* or *E. coli*. The antibacterial activities of ZnO, ZnO-TA, and ZnO-TA-Ag against *S. aureus* were significantly better than that of HA, with MICs of 0.625, 0.313, and 0.156 mg mL^{-1}, respectively (Figure 6A and Figure S4, Supporting Information). The antibacterial activities of ZnO, ZnO-TA, and ZnO-TA-Ag against *E. coli* were much weaker than those against *S. aureus*, with MICs of 2.500, 0.625, and 0.625 mg mL^{-1}, respectively (Figure 6B and Figure S4, Supporting Information). Images of bacterial colonies after 1 day's incubation on agar plates containing different concentrations' HA, ZnO, ZnO-TA, and ZnO-TA-Ag are shown in

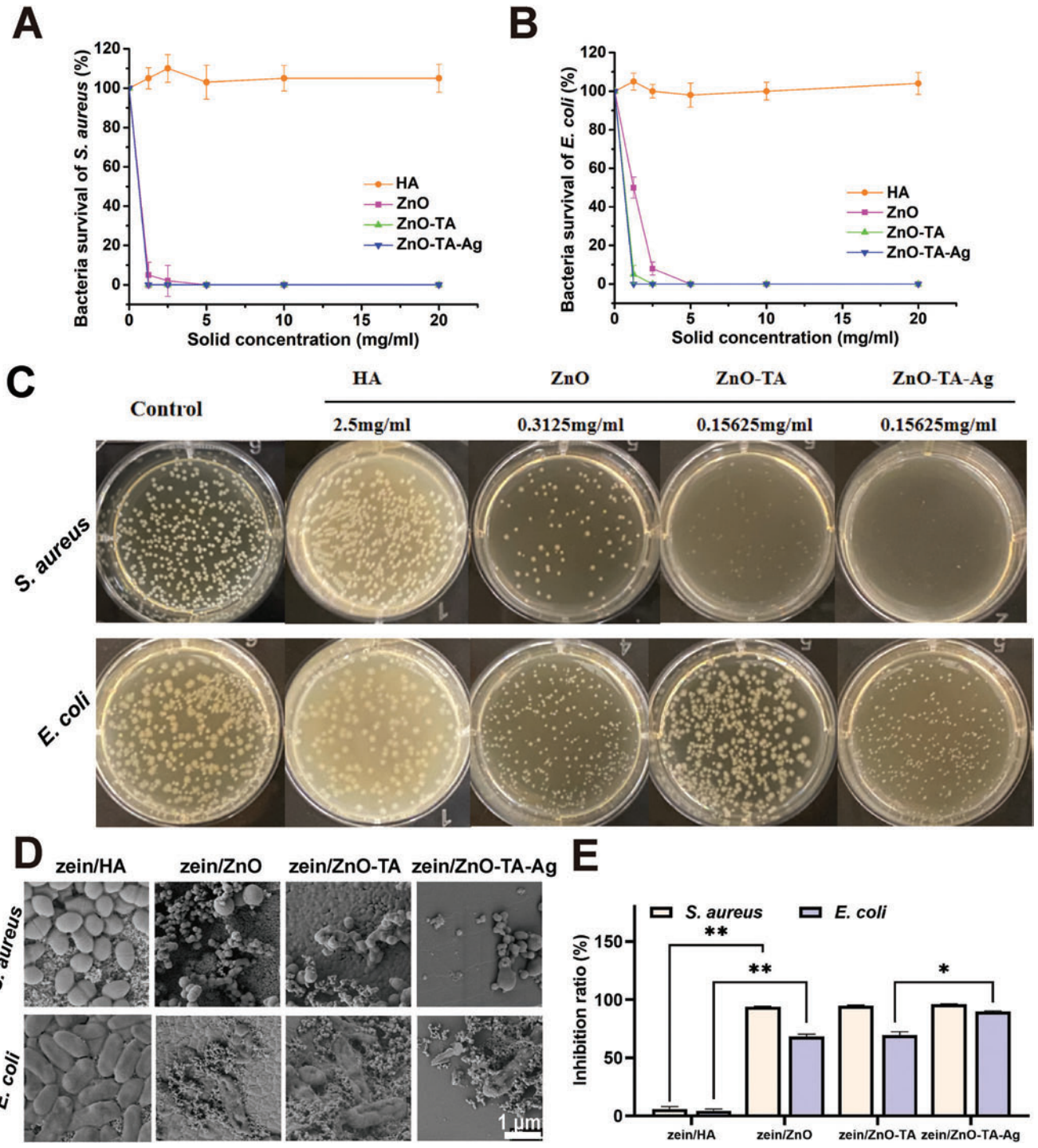

Figure 6. In vitro antibacterial study results of modified ZnOs and their composites: bacteria survivals on agar plates with different concentrations of HA, ZnO, ZnO-TA, and ZnO-TA-Ag against A) *Staphylococcus aureus* (*S. aureus*) and B) *Escherichia coli* (*E. coli*) ($n = 3$); C) representative bacteria colony images of agar plates containing HA, ZnO, ZnO-TA, and ZnO-TA-Ag; D) representative bacteria SEM images of bacteria contact killing tests after direct exploring to different composite disks for 24 h and E) the calculated bacterial inhibition ratios against *S. aureus* and *E. coli* ($n = 3$). $^{*}p < 0.05$, $^{**}p < 0.01$.

Figure 6C. These results confirmed the strong antibacterial activity of ZnO-TA and ZnO-TA-Ag, especially ZnO-TA-Ag, against Gram-positive bacteria. The relatively better antibacterial activities of ZnO-TA and ZnO-TA-Ag may be attributed to the faster Zn^{2+} ($\pm Ag^{+}$) releasing rates of TA modified ZnOs as well as the application of dual-metal (Zn and Ag) antibacterial mechanism.

The antibacterial activity of the composite disks (Φ15 mm × 1 mm) was evaluated by directly exposing them to 1 mL bacterial suspensions of *S. aureus* or *E. coli* ($\approx 1 \times 10^6$ colony-forming units (CFUs) mL^{-1} for 24 h before OD value measurement to obtain the bacterial inhibition ratios; the bacterial morphology was observed by SEM. As shown in Figure 6D, after direct exploration of the composite disks for 24 h, compared with that in zein/HA group, the number of live bacteria was greatly reduced in the Zn-based composite groups, and the morphology of the bacteria shrunk, confirming the strong antibacterial efficacy of all Zn-based composites. All zein/ZnO, zein/ZnO-TA, and zein/ZnO-TA-Ag groups achieved 90%–95% of *S. aureus* after 24 h, which was significantly higher than that of the zein/HA group (≈10%) (Figure 6E). Although the antibacterial activities of zein/ZnO, zein/ZnO-TA, and zein/ZnO-TA-Ag against *E. coli* were much weaker than those against *S. aureus*, the bacterial inhibition ratios against *E. coli* still ranged from 75% to 85% after 24 h, with zein/ZnO-TA-Ag showing the highest inhibition (≈85%) (Figure 6E). These results further confirmed the strong antibacterial ability of zein/ZnO, zein/ZnO-TA, and zein/ZnO-TA-Ag, especially that of the latter two with TA modification, which may be attributed to the fast release of Zn^{2+} ($\pm Ag^{+}$) from TA modified ZnOs and the antibacterial activity possessed by TA.[6,20b,23] The inclusion of Ag NPs further enhanced their antibacterial ability owing to the strong antibacterial activity of Ag^{+} and the application of dual-metal antimicrobial mechanisms.

2.7. In Vivo Study Using the Infected Femoral Condyle Defect Model on Rats

To evaluate the in vivo infected bone defect repair efficacy of the composites containing ZnO-TA and ZnO-TA-Ag, the porous MP scaffolds of zein/ZnO, zein/ZnO-TA and zein/ZnO-TA-Ag (porosity: 80%; pore size: 250–425 μm; the morphology of the scaffold before grinding is shown in Figure S5B, Supporting Information) were fabricated and used to treat the created infected femoral condyle defect on rats (Figure S5A, Supporting Information), with the untreated infected defect as blank control. After implantation of the porous composite MP scaffolds into the infected femoral condylar defects of SD rats for 72 h, the rats were euthanized, and the bone tissues surrounding the treated defects were collected and crushed with ultrasound, followed by rinsing with 1 mL of sterile PBS and bacterial growth on agar plates for 24 h before colony counting. As shown in Figure S5C, Supporting Information, the number of bacteria colonies was lower in the composite scaffold groups than in the control group, and the bacterial survival ratios of the zein/ZnO, zein/ZnO-TA, and zein/ZnO-TA-Ag groups were 8.83%, 8.51%, and 1.15%, respectively, which were significantly lower than that of the control group (100%) (Figure S5D, Supporting Information). The in vivo antibacterial results confirmed the strong antibacterial activity of the Zn-based biomaterials, especially when TA and Ag NPs were introduced into the modified ZnO, in agreement with the in vitro antibacterial results.

After implantation of the zein/ZnO, zein/ZnO-TA, and zein/ZnO-TA-Ag composite MP scaffolds for 4, 8, and 12 weeks, the bone tissues surrounding the infected rat femoral condyle defects were harvested for micro-CT analysis. As shown in the reconstructed 2D micro-CT images of the cross-sectional locations (**Figure 7**A), the bone defect sites were filled with the implanted composite and new bone tissue for all three composite groups, with the new bone shown in gray and the implanted composite in yellow. The mineral contents of the Zn-based composite groups were obviously higher than those of the control groups at 4, 8, and 12 weeks after operation. The bone mineral density (BMD) results (Figure 7B) revealed that the composite groups had significantly higher BMDs than the control group at all three time points, and the bone volume fractions (BV/TVs) showed the same trend (Figure 7C). However, the BMDs and BV/TV of the three Zn-based composite groups did not differ significantly (Figure 7B,C). This may be attributed to the faster in vivo degradation of zein/ZnO-TA and zein/ZnO-TA-Ag than that of zein/ZnO, which was further confirmed in the sagittal and coronal micro-CT images shown in Figure 7D. These results indicate that the osteogenic properties were not affected when TA and Ag NPs were incorporated into the modified ZnO, and the porous structure along with the degradation of Zn-based composites, created cavities for new bone growth.

To further investigate the osteoconductive and osteoinductive properties, histological (H&E and Masson's trichrome) and osteocalcin (OCN) and Runx2 immunohistochemical staining was performed on sections of decalcified bone tissues harvested at preset time points (4, 8, and 12 weeks). In the H&E stained images (**Figure 8**A), no severe inflammatory response within or around the implanted material was observed at any the three time points. In the control group, only a small amount of new bone formation at the edge of the defect was observed at week 4, and the new bone trabeculae had not yet filled the entire defect area by week 12 (Figure 8A), which was also confirmed from Masson's trichrome staining images (Figure 8A) and the corresponding collagen deposition contents of the control group (Figure 8B). All the three composite groups showed significantly better new bone growth and collagen deposition compared with the control group: at week 4, the edges of the defect in the composite groups partially degraded and internal new bone growth could be observed; at week 8, the newly formed bone filled almost the entire defect and encapsulated the implant material, and the morphology of the new bone trabeculae was also similar to that of the autologous bone (Figure 8A,B). At week 12, defects in the three composite groups healed almost completely. Comparing to zein/ZnO group, zein/ZnO-TA, and zein/ZnO-TA-Ag groups exhibited significantly ($p < 0.05$) improved collagen deposition, especially at week 4 (Figure 8B), indicating superior osteoconductivity compared with that of pure ZnO-containing composite. Runx2 is an early indicator of osteogenic differentiation during bone repair, while OCN is a marker of osteoblast maturation. As shown in Figure 8C–E, for all groups, OCN expression levels increased from week 4 to week 12, whereas the Runx2 expression levels increased from week 4 to week 8, and decreased at week 12. The expression levels of OCN and Runx2 in the three composite groups were significantly higher ($p < 0.05$ or 0.01) than that in the control group

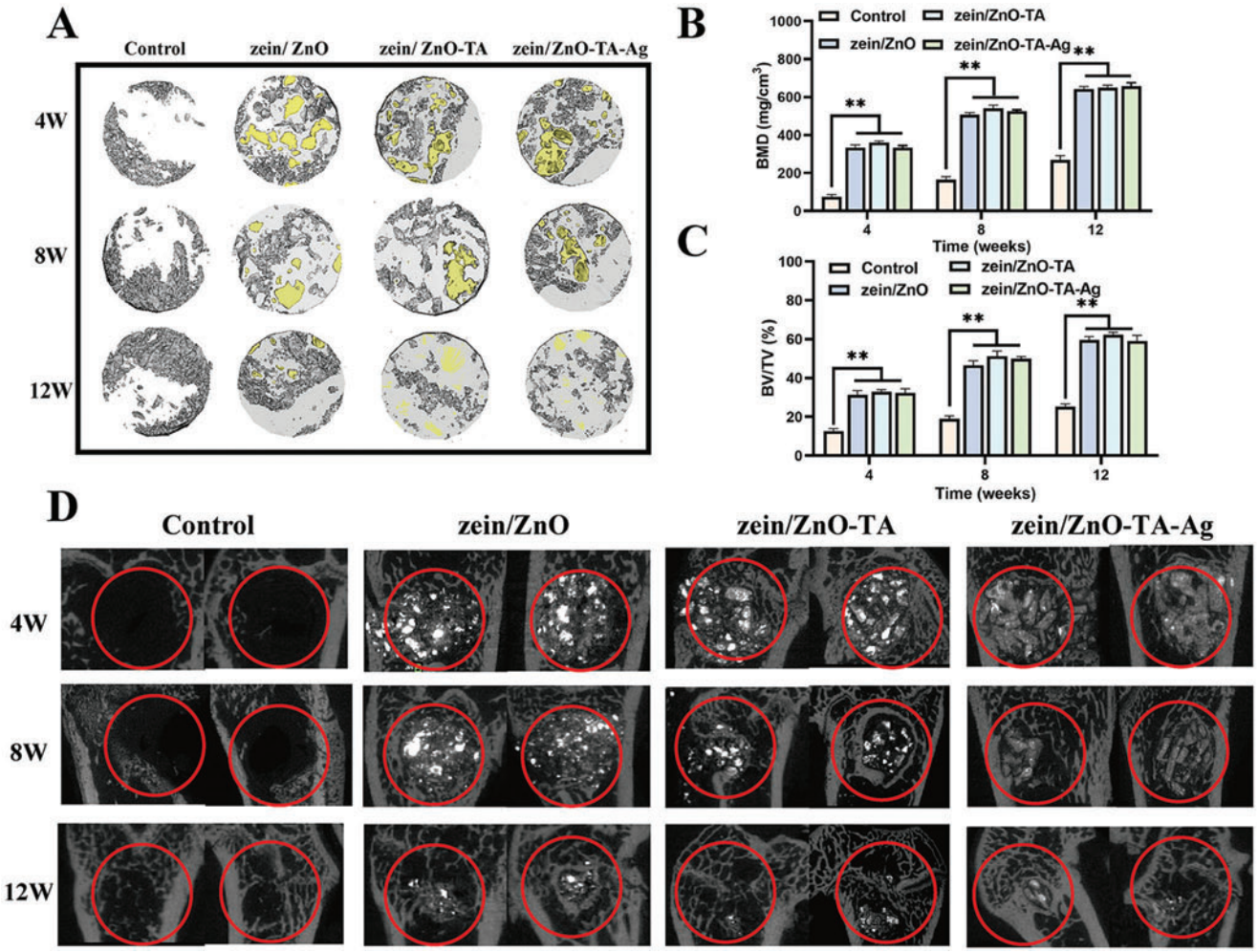

Figure 7. Micro-CT analysis results: A) Representative micro-CT images of the harvested bone surrounding the tissues femoral condyle defects 4, 8, and 12 weeks after operation, and the corresponding quantitative results of B) bone mineral densities (BMDs) and C) bone volume fractions (BV/TVs); D) the representative sagittal and coronal micro-CT images of the defect sites 4, 8, and 12 weeks after operation ($n = 6$). $^{**}p < 0.01$, "ns" represents no significant difference.

at all three time points (except week 12 for Runx2; Figure 8D,E). Compared to OCN, the increase in the expression of Runx2 in the composite groups, especially in the zein/ZnO-TA and zein/ZnO-TA-Ag groups, seemed more obvious at an earlier stage (weeks 4 to 8), which contributed to the significant difference in bone mass growth between the composite and control groups (Figure 7). Furthermore, there was a "snowball" effect on new bone formation, so although the expression of Runx2 decreased with osteoblast ossification at week 12, the expression levels of OCN were still maintained at week 12, reflecting the continual maturation of new bone (Figure 8D,E). These results further proved the favorable osteoconductivity and osteoinductivity of the Zn-based composites for treating infected bone defects, especially when TA and Ag NPs were introduced because the TA bulk modification of ZnO tremendously accelerated Zn^{2+} release, and the inclusion of Ag NPs enhanced antibacterial activity. In our previous study, a better antibacterial capability was proved could enhance osteogenesis in repairing infected bone defects.[2b]

The in vivo immunomodulatory and anti-inflammatory activities of zein/ZnO-TA and zein/ZnO-TA-Ag were investigated by immunofluorescence and immunohistochemical staining to better understand their osteogenesis promotion efficacy. For immunofluorescence staining, the surface markers CD86, representing pro-inflammatory M1 macrophages, and CD206, representing anti-inflammatory M2 macrophages, were used for co-staining. As shown in **Figure 9**A, the number of CD86 positive cells was obviously higher than that of CD206 positive cells at week 4, especially in the control group, suggesting that CD86 positive M1 macrophages predominantly mediate the bacterial immune process in the early stages of implantation. Although the introduction of Zn-based composites did not alter this physiological process, the inflammatory response was significantly reduced owing to the strong antibacterial activity of the Zn-based composites. As time progressed, at week 8, the number of CD86 positive cells decreased in all groups and almost disappeared at week 12, whereas the number of CD206 positive cells showed an increas-

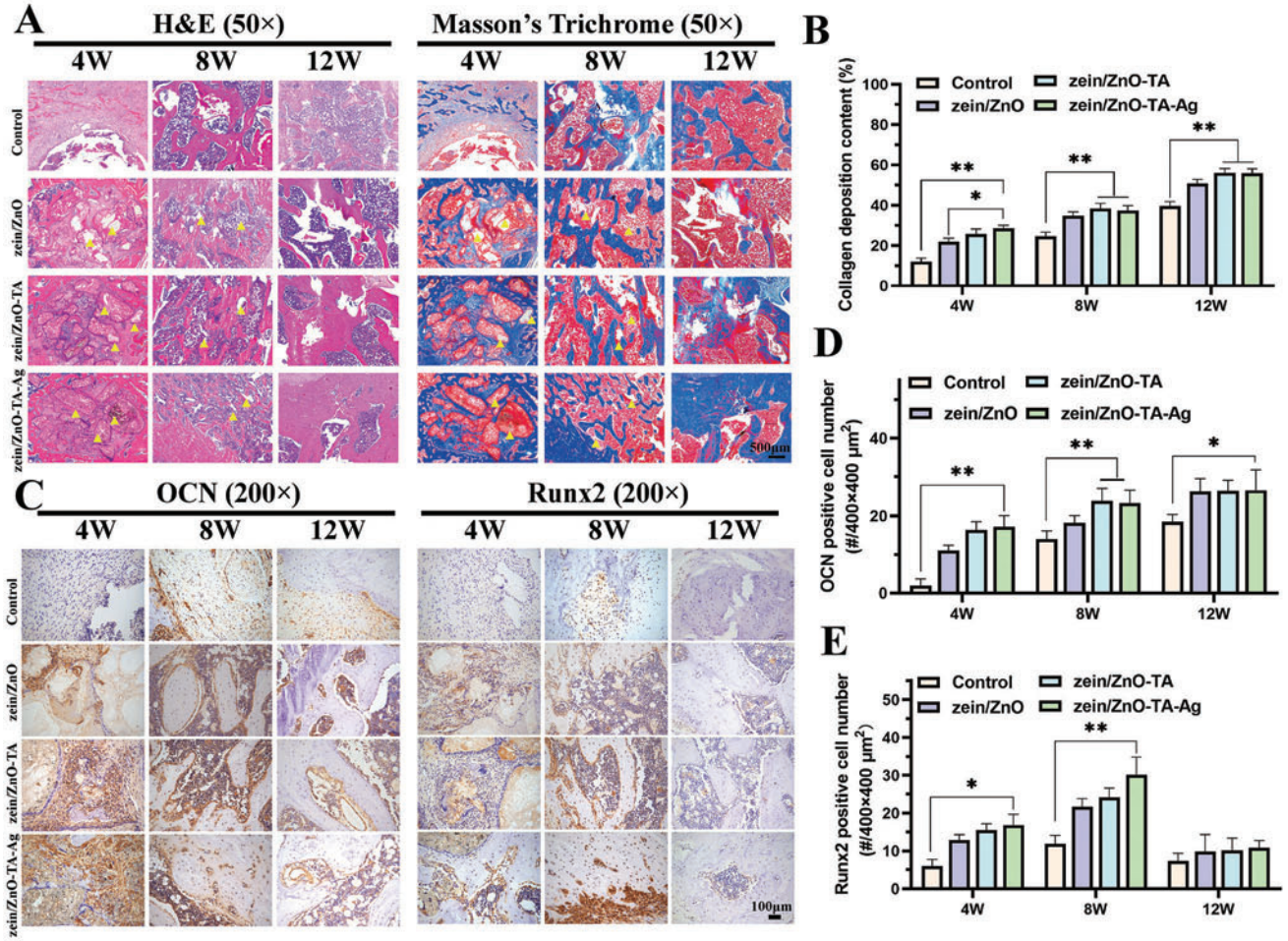

Figure 8. Histological and immunohistochemical staining results: A) hematoxylin and eosin (H&E) and Masson's trichrome staining images (the residual materials are labeled by yellow triangles) and B) the calculated collagen deposition contents of the decalcified bone tissue sections surrounding the defect for different groups 4, 8, and 12 weeks after operation ($n = 3$); C) osteocalcin (OCN) and Runx2 immunohistochemical staining images and the corresponding quantitative results of D) OCN and E) Runx2 (n = 4). *$p < 0.05$, **$p < 0.01$, "ns" represents no significant difference.

ing trend (Figure 9A); the Zn-based composite groups, especially the ones with TA modified ZnO, showed a significantly higher ($p < 0.01$ for zein/ZnO-TA-Ag, and $p < 0.05$ for zein/ZnO) number of CD206 positive cells than the control group (Figure 9C), consistent with the in vitro immunomodulatory results of zein/ZnO-TA and zein/ZnO-TA-Ag (Figure 5). These results revealed that TA bulk modification and the inclusion of Ag NPs in ZnO could promote the immunomodulatory ability of ZnO-based biomaterials by further promoting the polarization of macrophages toward anti-inflammatory M2 phenotype in vivo, proving the superiority of TA (± Ag NPs) modified ZnO in providing a favorable microenvironment for new bone formation. Moreover, the inflammatory response (using interleukin-1β (IL-1β) as the representative biomarker) was also assessed to further investigate the anti-inflammatory activity of zein/ZnO-TA and zein/ZnO-TA-Ag. As shown in the representative IL-1β immunohistochemical staining images (Figure 9B), the expression level of IL-1β in the control group was significantly higher than that in the composite group at week 4 ($p < 0.01$ comparing with zein/ZnO-TA-Ag), with the expression level of IL-1β in the zein/ZnO-TA-Ag group being the lowest (Figure 9D), indicating the superior anti-inflammatory activity of zein/ZnO-TA-Ag. The expression levels of IL-1β in all groups decayed with time progress, but the composite groups (especially the zein/ZnO-TA-Ag group) exhibited significantly less IL-1β expression ($p < 0.01$ at week 8 and $p < 0.05$ at week 12 for the zein/ZnO-TA-Ag group) than the control group (Figure 9B,D). It is worth noting that at week 4, although more ROS might be produced by zein/ZnO-TA-Ag than zein/ZnO-TA because of Ag NPs, the zein/ZnO-TA-Ag group showed significantly less IL-1β expression ($p < 0.05$) than the zein/ZnO-TA group (Figure 9D). This may be attributed to the fact that the better antibacterial ability of zein/ZnO-TA-Ag could kill more bacteria, thus contributing to a reduction in the endogenous ROS produced by bacterial infection. The results suggest that the introduction of TA + Ag NPs into modified ZnO further enhances the immunomodulatory and anti-inflammatory activity of ZnO, which is beneficial for providing a favorable osteogenic microenvironment, especially when bone infection is involved.

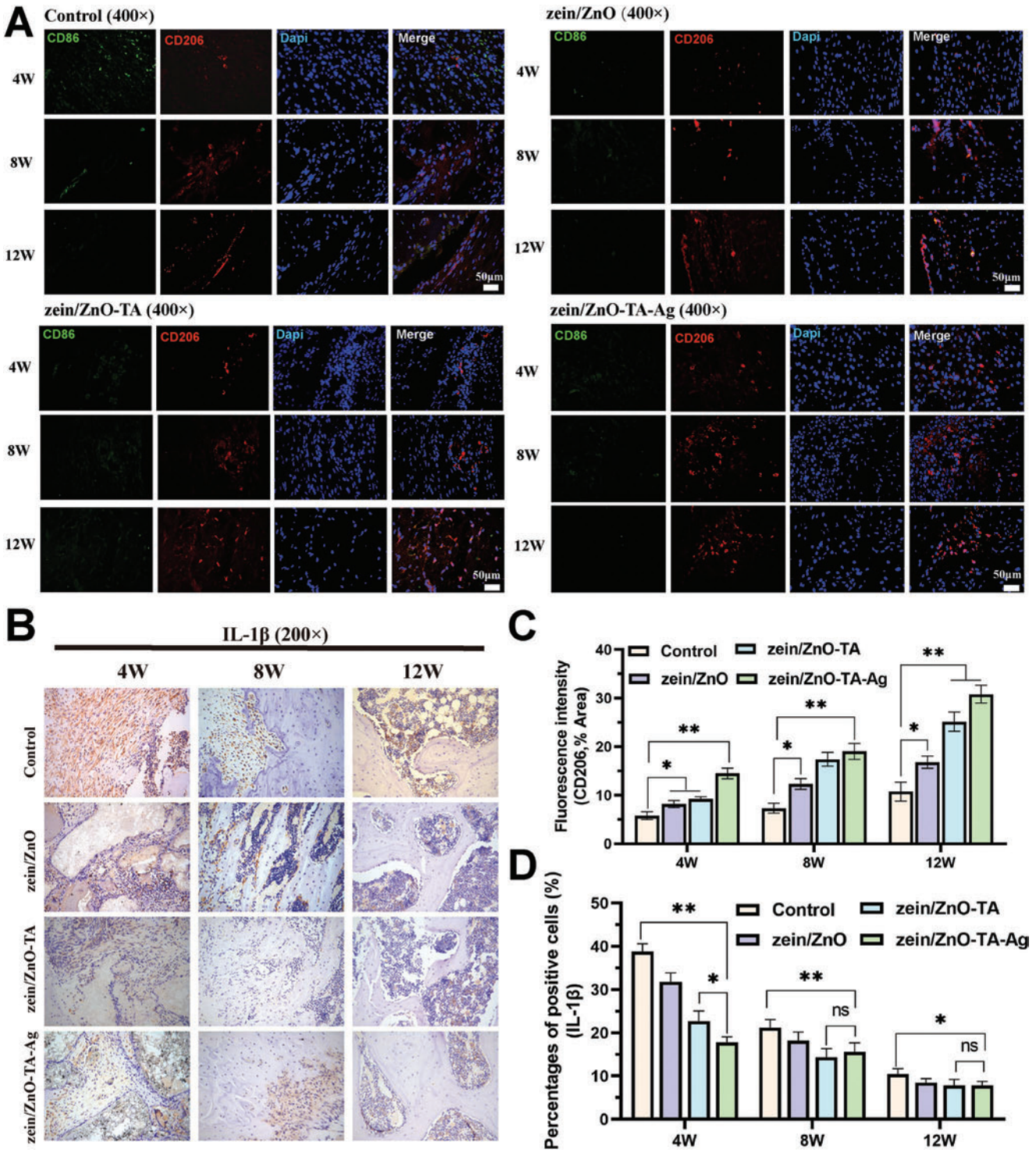

Figure 9. The immunofluorescence (CD86 and CD206) and IL-1β immunohistochemical staining results: A) immunofluorescence (CD86 and CD206), B) IL-1β immunohistochemical staining images 4, 8, and 12 weeks after composite implantation, and C) the calculated fluorescence intensities for CD206 ($n = 4$), D) the calculated percentages of IL-1β positive cells ($n = 4$). *$p < 0.05$, **$p < 0.01$, "ns" represents no significant difference.

The inclusion of tannin in the bulk modification significantly accelerated the release of Zn^{2+} and Ag^{+} from the zein/ZnO-TA-Ag composite scaffolds, providing an effective antibacterial effect to control bacterial infection. Both in vitro and in vivo antibacterial experiments confirmed sufficient antibacterial activity of the zein/ZnO-TA-Ag scaffolds. Simultaneously, synchronously-released TA molecules (with strong anti-oxidant ability) could scavenge endogenous ROS and ROS produced by antibacterial Zn^{2+} and Ag^{+}, providing enhanced immunomodulatory activity compared to that of pure ZnO in promoting M2 polarization of macrophages, which, together with the favorable osteogenic property of Zn^{2+}, could significantly promotes osteogenesis. The Zn-based tannin-modified composite MP scaffolds exhibited balanced antibacterial activity and osteogenic ability, which are beneficial for infection control and bone regeneration in infected bone defects.

3. Conclusion

In summary, a facile one-pot hydrothermal reaction of Zn acetate in the presence of TA, with or without $AgNO_3$, was used to synthesize a TA or TA and Ag NPs bulk-modified ZnO (ZnO-TA or ZnO-TA-Ag), which is further composited with zein to construct a series of novel inorganic–organic hybrid Zn-based tannin-modified composite MP scaffolds for infected bone defect repair. Although the crystalline structure of ZnO did not change, the introduction of TA-Zn^{2+} coordination bonds is believed to significantly change the connection mode between the ZnO crystals, and thus, the morphology of the modified ZnO. ZnO-TA particles are small but stacked cauliflower-like nanoparticles and ZnO-TA-Ag particles are in micro-sized (≈3 µm) spherical morphology. Moreover, bulk TA modification significantly accelerated the Zn^{2+} release (>100 times that of pure ZnO). This not only suppresses potential postoperative bacterial infection along with the released Ag+ from ZnO-TA-Ag but also enhances osteogenesis by promoting the osteogenic differentiation of bone marrow mesenchymal stem cells (BMSCs), enhancing endogenous citric acid production by osteoblasts and subsequent mineralization and providing considerable immunomodulatory activity to promote the M2 polarization of macrophages. Simultaneously, synchronously-released TA molecules can scavenge endogenous ROS and ROS produced by antibacterial metals, further enhancing the immunomodulatory activity of Zn^{2+} and providing superior anti-inflammatory properties. Favorable in vivo bacterial control and osteogenesis-promoting performance of the newly developed Zn-based tannin-modified composite scaffolds were confirmed in an infected femoral condyle defect model. Facile tannin modification confers balanced antibacterial and osteogenic properties to Zn-based tannin-modified composite scaffolds. The design strategy can be universally expanded to other tissue engineering areas where complicated and harsh microenvironments, such as bacterial infection or high ROS levels, are involved and can inspire more innovations in regenerative medicine and biomaterials.

4. Experimental Section

Materials: Tannic acid (TA, Mw = 1701.2 Da), zinc acetate ($Zn(CH_3COOH)_2$), zein and 2, 2-diphenyl-1-picrylhydrazyl (DPPH, 96%) were purchased from Macklin Reagent. Silver nitrate ($AgNO_3$) and hydroxyapatite (HA) were purchased from Sigma-Aldrich. All chemicals were used without further purification.

General Measurements: Fourier transform infrared (FTIR) spectra were measured on a Thermo Scientific Nicolet-iS10 FTIR spectrometer. X-ray diffraction (XRD) measurements of modified and unmodified ZnO as well as TA samples were conducted on a Bruker D8 X-ray powder diffractometer (Cu Kα radiation, 45 kV, 40 mA) with the detection range from 5 to 80 degrees. TGA experiments were analyzed using a thermogravimetric analyzer (NETZSCH STA 449F3, Nai, Germany) with a heating rate of 10 °C min^{-1} under N_2 atmosphere. Scanning electron microscopy (SEM) images and energy dispersive spectrometer (EDS) data were obtained using a ZEISS Sigma 300 (Germany).

Synthesis and Characterizations of ZnO and Modified ZnO: ZnO, TA modified ZnO (ZnO-TA) as well as TA and Ag NPs modified ZnO (ZnO-TA-Ag) were synthesized via a hydrothermal reaction method. For the synthesis of ZnO, 2.5 g zinc acetate was charged into a 100 mL hydrothermal reactor containing 40 mL ethanol, the reactor was then sealed and heated at 120 °C for 12 h. The crude product was collected by centrifuge at 8000 rpm for 5 min, further washed with ethanol and then water for at least three times, respectively, followed by freeze-drying to obtain purified ZnO. ZnO-TA was synthesized through a similar process, but in the suspension of 2.5 g zinc acetate in 40 mL ethanol, additional 0.125 g TA was added. And for ZnO-TA-Ag, in the suspension of 2.5 g zinc acetate in 40 mL ethanol, 0.125 g TA and 0.125 g silver nitrate were added. The chemical and physical properties, thermal stability and morphology of ZnO, ZnO-TA and ZnO-TA-Ag were characterized by FTIR, XRD, TGA, and SEM, and the results are shown in Figure 1A–C.

Release Experiments of Metal Ions: To investigate the release behavior of Zn^{2+} from ZnO-TA or Zn^{2+} and Ag^{+} from ZnO-TA-Ag, 0.1 g ZnO-TA or ZnO-TA-Ag was charged into a dialysis tube (with a molecular weight cut-off (MWCO) of 500 Da) and put in 50 mL PBS (pH 7.4) solution in a covered glass vial, and incubated in an oscillating incubator at 37 °C. At each pre-set time point, 1.0 mL solution was taken from the glass vial (1.0 mL fresh PBS was put back to the glass vial to keep the volume consistent), and the amount of Zn^{2+}/Ag^{+} released was measured by inductively coupled plasma mass spectrometry (ICP-MS, ICPMS-2030, Shimadzu, Japan). Four parallels were set for each sample and the results were averaged.

Fabrication of the Nonporous Composites and Porous MP Scaffolds of Modified ZnO and Zein: The nonporous composites of zein with HA, ZnO, ZnO-TA, and ZnO-TA-Ag were fabricated for degradation, biomineralization, antimicrobial and cell proliferation studies. First, 6 g HA, ZnO, ZnO-TA or ZnO-TA-Ag was mixed with 10 g 25 wt% zein solution in 90% ethanol (v(ethanol)/v(water) = 90/10), the mixture was uniformly mixed, casted in a Teflon mold, followed by solvent evaporation and thermal crosslinking in an oven at 120 °C, 3 days and 120 °C vacuum for another day to obtain nonporous zein/HA 60 wt%, zein/ ZnO-TA 60 wt%, or zein/ZnO-TA-Ag 60 wt% composites (60 wt% was the weight ratio of modified ZnO or HA to the total dry weight). Composite disks for degradation study were made into 7 mm in diameter and 0.5 mm in thickness.

Porous zein/HA (HA content: 60 wt%), zein/ZnO-TA (ZnO-TA content: 60 wt%) and zein/ZnO-TA-Ag (ZnO-TA-Ag content: 60 wt%) composite scaffolds with a porosity of 80% and pore size of 250–425 µm were also fabricated using the salt leaching method adapted from previous literatures.[10] Briefly, sieved sodium chloride (NaCl, salt) crystals (250–425 µm, 80 wt% to the total weight of salt, dry polymer and HA, ZnO-TA, or ZnO-TA-Ag) were added to preset amounts of HA, ZnO-TA or ZnO-TA-Ag and zein solution (25 wt% in 90% ethanol), and stirred to evaporate the solvent until the mixture became a viscous solid before being casted in cuboid Teflon molds. The dried scaffolds then thermal crosslinked at 120 °C, 3 days and 120 °C vacuum for another day. After crosslinking, salt was leached from the scaffolds in deionized water for at least 1 week followed by lyophilization. The obtained porous scaffolds were then grounded and sieved, to give MP scaffolds with sizes between 250 and 425 µm.

Degradation Study: For degradation studies, composite disks (Φ7 mm, 0.5 mm thickness) were placed in plastic tubes containing 10 mL of phosphate buffered saline (PBS, pH 7.4) and incubated at 37 °C. PBS was changed every 1 week. After preset incubation times, specimens were

washed thoroughly with water for at least four times to remove residual salt before freeze-drying. Mass loss was calculated by Equation (1). Here W_0 and W_1 are the initial weight and the weight after degradation, respectively. For each sample, at least five specimens were tested and the results were averaged.

$$\text{Mass Loss}\ (\%) = \frac{W_0 - W_1}{W_0} \times 100 \quad (1)$$

The pH values of the PBS buffer solutions after degradation were also measured.

Anti-Oxidant Property of the Modified ZnO: The anti-oxidant activity of ZnO, ZnO-TA, and ZnO-TA-Ag was assessed by the DPPH radical scavenging method. Typically, 2 mg sample was added to 3.0 mL DPPH (100 µmol L^{-1}) methanol solution. The mixture was incubated under dark for 15 min. Then a wavelength scan was performed with a UV–vis spectrophotometer (Shimadzu 2600i, Japan). The degradation rate of DPPH was calculated using Equation (2), where A_B and A_S are the absorbance of blank (DPPH + ethanol) and sample (DPPH + ethanol + sample), respectively.

$$\text{DPPH clearance rate} = \frac{A_B - A_S}{A_B} \times 100\% \quad (2)$$

A reactive oxygen species (ROS) assay (Solarbio, Beijing) on ZnO, ZnO-TA and ZnO-TA-Ag was also conducted to investigate their intracellular ROS scavenging ability. An appropriate amount of rat bone mesenchymal stem cells (rBMSCs, ATCC PCS-500-012TM, 5–10 passage) were seeded in the wells of 96-well and 24-well plates, respectively, and incubated in complete Dulbecco's modified eagle's medium (DMEM) containing 10% (v/v) fetal bovine serum (FBS) and 1% (v/v) antibiotic antifungal solution (100×) at 37 °C for 12 h. After adding the material suspension (100 µg mL^{-1}) to the medium and incubated for 2–4 h, the ROS UP reagent (reactive oxygen species assay kit, Beyotime, S0033S, 1:1000) was added and the mixture was allowed to react for 30 min, then the medium was discarded, the cells was washed softly with DMEM twice, followed by incubating with DCFH-DA assay reagent (1:1000) for ≈20–30 min before observation with an inverted fluorescence microscope (Leica DMI4000 B; Leica Microsystems GmbH, Wetzlar, Germany; for 24-well plates). Quantitative assay using fluorescent enzyme marker (pay attention to avoid light during operation) was also conducted for the 96-well plates. Untreated cells were used as negative control, and Ros up-treated cells (without sample) were used as a positive control.

Biomineralization: The in vitro biomineralization ability of the composites of zein and modified ZnO was evaluated with the crosslinked nonporous composite disks (Φ15 mm × 0.5 mm) of zein/ZnO 60 wt%, zein/ZnO-TA 60 wt%, and zein/ZnO-TA-Ag 60 wt%. The zein/HA 60 wt% composite disks were used as control. To accelerate the mineralization process, the samples were immersed in 10 mL 5× simulated body fluid (SBF-5×) and incubated at 37 °C for 10 days. Half of the SBF-5× solution was replaced with fresh SBF-5× solution every other day. At each preset time point, the specimens (n = 5) were removed from the solution, gently washed with deionized water to remove inorganic ions from the surface of the specimens, and then air dried. Next, the specimens were sputter coated with gold (5 nm thick) and observed by scanning electron microscopy (SEM, ZEISS Sigma 300).

Cytocompatibility Study of Modified ZnO and Their Composites with Zein: The cytocompatibility of zinc ions (using $ZnCl_2$ with different concentrations), inorganic materials (ZnO, ZnO-TA, and ZnO-TA-Ag) and their composites with zein (zein/ZnO 60 wt%, zein/ZnO-TA 60 wt%, and zein/ZnO-TA-Ag 60 wt%, using PLGA as control) was evaluated using rBMSCs. Cells were cultured in complete DMEM containing 10% (v/v) fetal bovine serum (FBS) and 1% (v/v) antibiotic antifungal solution (100×), and incubated at 37 °C, 5% CO_2, and 95% relative humidity.

To assess the cytotoxicity of ZnO, ZnO-TA, and ZnO-TA-Ag, 100 µL rBMSCs suspension (3×10^4 cells mL^{-1}) in complete DMEM was seeded in each well of 96-well plates and cultured overnight, then 10 µL ZnO, ZnO-TA, or ZnO-TA-Ag dispersion with different concentrations (400, 200, 100, 50, 20, 10, and 5 µg mL^{-1}) in sterile PBS was added to each well of 96-well plates, and the cells were cultured for another day before conducting CCK-8 assay according to the manufacturer's protocol. The rBMSCs cultured in blank DMEM were used as control. For each group, at least 6 parallels were set and the results were averaged.

The cytocompatibility of composites was studied using the complete degradation products of the composites. PLGA (LA/GA = 50/50, Mw ≈60 kDa, purchased from Alladin) was used as control. Briefly, 1.0 g composite sample or PLGA was completely degraded in 1.0 mol L^{-1} NaOH solution to obtain 1× degradation product solution, which was neutralized to pH 7.4 and sterilized by passing through a 0.22 µm Teflon filter. The sterilized 1× degradation product solutions were then diluted 10 or 100 times with sterile PBS to give 10× or 100× degradation product dilutions. For each well of 96-well plates, 100 µL rBMSCs suspension in complete DMEM (3×10^4 cells mL^{-1}) were seeded and incubated overnight, then 10 µL degradation product in different dilutions was added to the well, and the cells were cultured for one more day before being quantified with CCK-8 assay. For each cohort, at least six parallels were set and the results were averaged. The rBMSCs treated with 10× degradation products were further stained by a Live/Dead Viability/Cytotoxicity Kit (Invitrogen, molecular probes, Eugene, OR) and the morphology of rBMSCs was observed with an inverted fluorescence microscope (Leica DMI4000 B; Leica Microsystems GmbH, Wetzlar, Germany).

Osteogenic Differentiation Study: The effect of Zn^{2+} at different concentrations to the osteogenic differentiation of rBMSCs, the endogenous citric acid (CA) production, the ALP expression, and the mineralization was studied. Briefly, after seeding rBMSCs in the wells of 24-well plates, $ZnCl_2$ with different concentrations in osteogenic media (complete DMEM supplemented with 10^{-7} M dexamethasone, 10^{-2} M β-glycerophosphate, and 50 mM L-ascorbic acid) was added after 1 day's incubation. The medium was changed every 2 days. At day 7 and 14, ALP assay and the CA production tests were conducted, and the cells were also stained with ALP and Alizarin red staining kit followed by microscopic observation with an inverted fluorescence microscope (Leica DMI4000 B; Leica Microsystems GmbH, Wetzlar, Germany).

Western blot was also used to verify the expression of osteogenic-related proteins (ALP and Runx2) after the intervention of composite degradation products on osteoblasts. When the cells were treated, the cell plates were removed from the incubator, cell growth viability was observed, excess complete medium was aspirated with a sterile gun, and the cells were washed with sterile PBS solution; after washing, protein lysate was added to the wells, and the completely lysed solution was transferred to an Eppendorf (EP) micro test tube and denatured by heating for 10 min; after centrifuging at 10 000 rpm for 5 min to remove cell debris, the supernatant was used for Western blotting experiment following the standard protocol.

Immunomodulatory Ability of Modified ZnO and the Composites: The cytotoxicity of ZnO, ZnO-TA, and ZnO-TA-Ag against RAW264.7 was assessed using the CCK-8 assay. Cells were intervened by adding different concentrations of inorganic components to the medium and cultured after 24 h. The absorbances of each group were measured according to the instructions of the CCK-8 kit, and for each group, at least 6 samples were measured and the results were averaged. The ratio of M1 and M2 macrophages was determined using flow cytometry. The flow antibody used in this test was purchased from eBioscience. The RAW264.7 cell line was selected to be seeded into 12-well plates, and the complete degradation product (100 µL) of the composite (zein/ZnO, zein/ZnO-TA, and zein/ZnO-TA-Ag) was added to the medium, and the cells were treated with 100 ng mL^{-1} lipopolysaccharide (LPS) per well to stimulate the polarization of the cells. After 24 h' incubation, the cells were detached, centrifuged and stained with aliquot phycocyanin (APC)-conjugated CD86 and phycoerythrin (PE)-conjugated CD206 for 1 h under dark. The unbound free antibody was washed three times by PBS. Finally, 150 µL cell suspension was added to each well of 96-well plates and assayed by Guava flow cytometry (Millipore, USA). Data were analyzed by Flowjo10.

In Vitro Antimicrobial Study: *S. aureus*, ATCC 6538TM and *E. coli*, ATCC 25922TM were used for antimicrobial study and cultured according to standard safety protocols. Tryptic soy broth (TSB) was used for *S. aureus*

culture and Luria-Bertani (LB) medium was used for *E. coli* culture. The mono-colony *S. aureus* and *E. coli* were incubated at 37 °C on a rotary shaker (150 rpm) overnight, and then diluted into desired concentrations before use.

Minimum Inhibitory Concentrations of Modified ZnO against Bacteria: The MICs of ZnO, ZnO-TA and ZnO-TA-Ag against *S. aureus* and *E. coli* were determined using an agar macrodilution method adapted from previous literature,[6,20d,24] HA was used as a control. Briefly, HA, ZnO, ZnO-TA, or ZnO-TA-Ag suspensions with preset concentrations (5, 2.5, 1.25, 0.625, and 0.3125 mg mL^{-1}) were made using deionized water and the corresponding agar mix for *S. aureus* (Tryptic soy agar) or for *E. coli* (LB broth and agar). The solutions were mixed in glass vials, covered with foil, and then autoclaved to sterilize the agar/particle mixtures, then the hot mixtures were placed in the wells (3 mL $well^{-1}$) of 6-well plates and allowed to solidify. Blank agar was used as control. After solidification, the bacterial suspension was evenly distributed in the wells of 6-well plates and excess medium was allowed to evaporate. The plates were then incubated at 37 °C for 24 h and the bacterial colonies were counted using ImageJ. Make sure that the colonies fell in a countable range of 25–250 CFUs $well^{-1}$ (CFU: colony forming units). For different bacteria, a standard curve of CFUs mL^{-1} versus optical density (OD) values at 600 nm was obtained first to roughly predict bacterial concentrations. Bacterial viability was calculated using Equation (3), here *N* is the number of bacterial colonies in the sample well and *N*c is the number of colonies in the blank well.

$$\text{Bacteria survival } (\%) = (N/N_c) \times 100 \tag{3}$$

For each particle concentration, at least 3 specimens were tested and the results averaged. For ZnO, ZnO-TA, and ZnO-TA-Ag, the obtained lowest concentration with no bacterial survival was determined as the MIC of the particle against the tested bacteria.

The antimicrobial performance of the zein/ZnO, zein/ZnO-TA, and zein/ZnO-TA-Ag composites (the contents of ZnO and modified ZnO were 60 wt% for all samples) was also evaluated by direct exposure to bacterial suspensions of *S. aureus* and *E. coli*. Composite disks (Φ15 mm × 0.5 mm) were placed into the wells of 24-well plates, then 1 mL bacterial suspension ($\approx 1 \times 10^6$ CFUs mL^{-1}) was added to each well. The discs of zein/HA and PLGA with the same size were used as positive and negative controls, respectively, while the blank samples contained only pure bacterial suspension. The bacterial suspensions were incubated at 37 °C for 24 h at a shaking speed of 150 rpm and then the bacterial suspensions were removed for OD measurement at 600 nm. The bacterial inhibition ratio was calculated by Equation (4).

$$\text{Bacterial inhibition ratio } (\%) = 100 - 100 \times \frac{A - A_0}{A_b - A_0} \tag{4}$$

Here A_0 is the initial OD value of the bacterial suspension, A is the OD value of the bacterial suspension of the composite sample after 24 h' incubation, and A_b is the OD value of the blank sample after 24 h' incubation. The bacteria grown on the surface of the composite disks were also fixed with 5% glutaraldehyde, gradiently dehydrated, coated with gold, and observed by SEM. The results are shown in Figure 3D–I.

Creation of Infected Femoral Condyle Defect Model on Rats and Porous MP Scaffolds Implantation: All surgical procedures as well as perioperative handling were conducted in accordance with protocols approved by the Animal Experimental Committee of Institute of Biological and Medical Engineering, Guangdong Academy of Sciences (Approval No. 2 021 013). 48 male Sprague Dawley (SD) rats at 8 weeks of age were purchased from the Medical Animal Experiment Center of Southern Medical University and randomly divided into four groups (12 rats per group): blank control group, zein/ZnO group, zein/ZnO-TA group, and zein/ZnO-TA-Ag group. The SD rats' right hind limbs were shaved with a shaver after anesthesia and then washed with povidone-iodine, and a 1.5–2.0 cm long incision was made on the lateral femoral condyle parallel to the long axis of the femoral stem, using the patellar ligament as reference. The skin and subcutaneous tissue were then incised to fully expose the lateral femoral condyle. A critical size bone defect (3.5 mm in diameter, 5 mm in depth) was created using an electric drill (Figure S5B, Supporting Information). After clearing the excess bone, 20 µL *S. aureus* suspension (1.0×10^8 CFUs mL^{-1}) was added to the defect site, and then the outer opening of the defect was closed using bone wax. After 10 days, the wound was opened and the bone wax was removed, the showed up of pus accumulation and acute periosteal reaction in the defect site indicated the successful creation of infected femoral condylar defect model. The bone wax was subsequently removed and the defect site was rinsed with sterile PBS before the implantation of Zein/ZnO, Zein/ZnO-TA, or Zein/ZnO-TA-Ag MP scaffolds, and a blank control with the infected bone defect being left untreated was also set. To determine the antimicrobial activity of the composite MP scaffolds in vivo, six SD rats were sacrificed for each group 72 h after material implantation, the treated femoral condylar defect site along with the surrounding bone tissue were harvested and crushed using ultrasound, then 1 mL sterile PBS was added and shaken for 10 min to ensure that the bacteria were shaken off (confirmed by microscopy). Then the collected bacterial suspension was diluted and casted on TSA agar gel in petri dishes, and incubated at 37 °C for 24 h, and the number of bacterial colonies was counted. The in vivo bacterial survival ratios of different samples were calculated by Equation (5).

$$\text{Bacterial survival ratio } (\%) = 100 \times \frac{N}{N_b} \tag{5}$$

Here *N* is the colony number of the sample, N_b is colony number of the blank control.

Micro-CT Analysis: At week 4, 8, and 12 post operation, SD rats were euthanized, the harvested femoral condyle specimens (6 for each sample) were fixed in 4% paraformaldehyde and stored at 4 °C for micro-CT and histology study. Micro-CT (Viva CT40; Scanco Medical AG, Bassersdorf, Switzerland) was conducted in an isolated bone mode to evaluate the bone regeneration in the defect area with the following settings: pixel size, 480 µm; slice thickness, 18 µm; number of slices: 210; rotation angle, 360°; X-ray voltage, low; artifact removal, lean; sync. scan, no; metal artifact reduction, no. The horizontal and vertical 2D images of the regenerated femoral condyle sections were reconstructed using Mimics software (version 20.0). A cylindrical space representing the volume of interest (VOI) was designated to evaluate new bone formation by calculating BMD and bone volume fraction (BV/TV) using Latheta software (Scanco Medical AG, Bassersdorf, Switzerland).

Histological Examination: At predetermined time points (4, 8, and 12 weeks after surgery), the treated bone tissues were harvested, decalcified with ethylenediaminetetraacetic acid (EDTA) decalcification solution (pH 7.4, Solarbio, China) at 37 °C for 1 month before conducting histological examinations according to a standard protocol. Longitudinal sections of 5 mm were cut at the epiphysis of interest using an SP2500 microtome (Leica Microsystems, Wetzlar, Germany). Hematoxylin and eosin (H&E) and Masson's trichrome staining, immunohistochemical staining of interleukin 1β (IL-1β), OCN, and Runx2, as well as immunofluorescence staining of macrophages (CD86 as the M1 surface marker and CD206 as the M2 surface marker) were performed, and observed with an inverted fluorescence microscope (Leica DMI4000 B; Leica Microsystems GmbH, Wetzlar, Germany). Semi-quantitative analysis of IL-1β, OCN, and Runx2 positively stained cells was also conducted using Image J.

Statistical Analysis: Statistical analysis was performed by using one-tailed Student's *t*-test by Statistical software (SPSS) when comparing two groups of data, and using analysis of variance (ANOVA) when comparing the means of more than two groups. Experimental results were expressed as mean ± standard deviation (SD). Differences were considered statistically significant when $p < 0.05$. * and ** represent $p < 0.05$ and $p < 0.01$, respectively.

Supporting Information

Supporting Information is available from the Wiley Online Library or from the author.

Acknowledgements

Y.Z., J.L., and L.L. contributed equally to this work. This work was supported by the Natural Science Foundation of China (Grant Nos. 82102545, 82272453, U21A2099, and 81974328), the Natural Science Foundation of Guangdong Extinguished Young Scholar Program (Grant No. 2022B1515020044), the Basic and Applied Basic Research Project of Guangzhou City (202201011774), and the Open Program from Guangdong Provincial Key Laboratory of Bone and Joint Degeneration Disease.

Conflict of Interest

The authors declare no conflict of interest.

Data Availability Statement

Research data are not shared.

Keywords

antimicrobial, immunomodulatory, osteogenic, silver, tannic acid, zinc oxide

Received: January 29, 2023
Revised: March 16, 2023
Published online:

[1] a) C. T. Johnson, J. A. Wroe, R. Agarwal, K. E. Martin, R. E. Guldberg, R. M. Donlan, L. F. Westblade, A. J. García, *Proc. Natl. Acad. Sci. USA* **2018**, *115*, E4960; b) E. F. Berbari, S. S. Kanj, T. J. Kowalski, R. O. Darouiche, A. F. Widmer, S. K. Schmitt, E. F. Hendershot, P. D. Holtom, P. M. Huddleston 3rd, G. W. Petermann, D. R. Osmon, *Clin. Infect. Dis.* **2015**, *61*, e26; c) J. Ye, B. Li, M. Li, Y. Zheng, S. Wu, Y. Han, *Acta Biomater.* **2020**, *107*, 313.

[2] a) M. Depypere, M. Morgenstern, R. Kuehl, E. Senneville, T. F. Moriarty, W. T. Obremskey, W. Zimmerli, A. Trampuz, K. Lagrou, W. J. Metsemakers, *Clin. Microbiol. Infect.* **2020**, *26*, 572; b) X. Tian, Z. Lu, C. Ma, M. Wu, C. Zhang, Y. Yuan, X. Yuan, D. Xie, C. Liu, J. Guo, *Mater. Sci. Eng., C* **2021**, *121*, 111807.

[3] E. A. Masters, R. P. Trombetta, K. L. de Mesy Bentley, B. F. Boyce, A. L. Gill, S. R. Gill, K. Nishitani, M. Ishikawa, Y. Morita, H. Ito, S. N. Bello-Irizarry, M. Ninomiya, J. D. Brodell, Jr., C. C. Lee, S. P. Hao, I. Oh, C. Xie, H. A. Awad, J. L. Daiss, J. R. Owen, S. L. Kates, E. M. Schwarz, G. Muthukrishnan, *Bone Res.* **2019**, *7*, 20.

[4] E. L. Cyphert, G. D. Learn, S. K. Hurley, C.-Y. Lu, H. A. von Recum, *Adv. Healthcare Mater.* **2018**, *7*, 1800812.

[5] a) C. T. Johnson, M. C. P. Sok, K. E. Martin, P. P. Kalelkar, J. D. Caplin, E. A. Botchwey, A. J. García, *Sci. Adv.* **2019**, *5*, eaaw1228; b) Z. A. Cheng, A. Alba-Perez, C. Gonzalez-Garcia, H. Donnelly, V. Llopis-Hernandez, V. Jayawarna, P. Childs, D. W. Shields, M. Cantini, L. Ruiz-Cantu, A. Reid, J. F. C. Windmill, E. S. Addison, S. Corr, W. G. Marshall, M. J. Dalby, M. Salmeron-Sanchez, *Adv. Sci.* **2019**, *6*, 1800361.

[6] J. Guo, X. Tian, D. Xie, K. Rahn, E. Gerhard, M. L. Kuzma, D. Zhou, C. Dong, X. Bai, Z. Lu, J. Yang, *Adv. Funct. Mater.* **2020**, *30*, 2002438.

[7] Z. Jia, P. Xiu, M. Li, X. Xu, Y. Shi, Y. Cheng, S. Wei, Y. Zheng, T. Xi, H. Cai, Z. Liu, *Biomaterials* **2016**, *75*, 203.

[8] A. Elrayah, W. Zhi, S. Feng, S. Al-Ezzi, H. Lei, J. Weng, *Materials* **2018**, *11*, 1516.

[9] a) W. Guan, L. Tan, X. Liu, Z. Cui, Y. Zheng, K. W. K. Yeung, D. Zheng, Y. Liang, Z. Li, S. Zhu, X. Wang, S. Wu, *Adv. Mater.* **2021**, *33*, 2006047; c) X. Jing, C. Xu, W. Su, Q. Ding, B. Ye, Y. Su, K. Yu, L. Zeng, X. Yang, Y. Qu, K. Chen, T. Sun, Z. Luo, X. Guo, *Adv. Healthcare Mater.* **2022**, *12*, 2201349.

[10] a) H. Yang, B. Jia, Z. Zhang, X. Qu, G. Li, W. Lin, D. Zhu, K. Dai, Y. Zheng, *Nat. Commun.* **2020**, *11*, 401; b) X. Qu, H. Yang, B. Jia, Z. Yu, Y. Zheng, K. Dai, *Acta Biomater.* **2020**, *117*, 400.

[11] X. Shen, Y. Zhang, P. Ma, L. Sutrisno, Z. Luo, Y. Hu, Y. Yu, B. Tao, C. Li, K. Cai, *Biomaterials* **2019**, *212*, 1.

[12] J. P. O'Connor, D. Kanjilal, M. Teitelbaum, S. S. Lin, J. A. Cottrell, *Materials* **2020**, *13*, 2211.

[13] A. S. Prasad, *Adv. Nutr.* **2013**, *4*, 176.

[14] X. Qu, H. Yang, Z. Yu, B. Jia, H. Qiao, Y. Zheng, K. Dai, *Bioact. Mater.* **2020**, *5*, 410.

[15] X. Fu, Y. Li, T. Huang, Z. Yu, K. Ma, M. Yang, Q. Liu, H. Pan, H. Wang, J. Wang, M. Guan, *Adv. Sci.* **2018**, *5*, 1700755.

[16] Y. Y. Hu, A. Rawal, K. Schmidt-Rohr, *Proc. Natl. Acad. Sci. USA* **2010**, *107*, 22425.

[17] a) L. C. Costello, R. B. Franklin, M. A. Reynolds, M. A. Chellaiah, *Open Bone J.* **2012**, *4*, 27; b) A. Lotsari, A. K. Rajasekharan, M. Halvarsson, M. Andersson, *Nat. Commun.* **2018**, *9*, 4170; c) C. Ma, X. Tian, J. P. Kim, D. Xie, X. Ao, D. Shan, Q. Lin, M. R. Hudock, X. Bai, J. Yang, *Proc. Natl. Acad. Sci. USA* **2018**, *115*, E11741.

[18] a) W. Liu, J. Li, M. Cheng, Q. Wang, K. W. K. Yeung, P. K. Chu, X. Zhang, *Adv. Sci.* **2018**, *5*, 1800749; b) I. Cockerill, Y. Su, J. H. Lee, D. Berman, M. L. Young, Y. Zheng, D. Zhu, *Nano Lett.* **2020**, *20*, 4594.

[19] a) A. Khader, T. L. Arinzeh, *Biotechnol. Bioeng.* **2020**, *117*, 194; b) Y. Xia, X. Fan, H. Yang, L. Li, C. He, C. Cheng, R. Haag, *Small* **2020**, *16*, e2003010.

[20] a) Y. Li, Y. Miao, L. Yang, Y. Zhao, K. Wu, Z. Lu, Z. Hu, J. Guo, *Adv. Sci.* **2022**, *9*, 2202684; b) K. Wu, M. Fu, Y. Zhao, E. Gerhard, Y. Li, J. Yang, J. Guo, *Bioact. Mater.* **2023**, *20*, 93; c) M. Fu, Y. Zhao, Y. Wang, Y. Li, M. Wu, Q. Liu, Z. Hou, Z. Lu, K. Wu, J. Guo, *Small* **2023**, *19*, 2205489; d) Y. Li, Y. Miao, L. Yang, G. Wang, M. Fu, Y. Wang, D. Fu, J. Huang, J. Wang, Z.-X. Fan, Z. Lu, J. Guo, Z. Hu, *Chem. Eng. J.* **2023**, *455*, 140572; e) M. J. Malone-Povolny, S. E. Maloney, M. H. Schoenfisch, *Adv. Healthcare Mater.* **2019**, *8*, 1801210; f) K. Wu, X. Wu, J. Guo, Y. Jiao, C. Zhou, *Adv. Healthcare Mater.* **2021**, *10*, 2100793.

[21] a) Z. Lu, J. Zhou, A. Wang, N. Wang, X. Yang, *J. Mater. Chem.* **2011**, *21*, 4161; b) X. Heng, M. Xiang, Z. Lu, C. Luo, *ACS Appl. Mater. Interfaces* **2014**, *6*, 8032.

[22] J. Guo, W. Sun, J. P. Kim, X. Lu, Q. Li, M. Lin, O. Mrowczynski, E. B. Rizk, J. Cheng, G. Qian, J. Yang, *Acta Biomater.* **2018**, *72*, 35.

[23] a) J. Guo, G. B. Kim, D. Shan, J. P. Kim, J. Hu, W. Wang, F. G. Hamad, G. Qian, E. B. Rizk, J. Yang, *Biomaterials* **2017**, *112*, 275; b) J. Guo, W. Wang, J. Hu, D. Xie, E. Gerhard, M. Nisic, D. Shan, G. Qian, S. Zheng, J. Yang, *Biomaterials* **2016**, *85*, 204; c) X. Lu, S. Shi, H. Li, E. Gerhard, Z. Lu, X. Tan, W. Li, K. M. Rahn, D. Xie, G. Xu, F. Zou, X. Bai, J. Guo, J. Yang, *Biomaterials* **2020**, *232*, 119719.

[24] a) G. M. Lee, S. Kim, E. M. Kim, E. Kim, S. Lee, E, L., H. H. Park, H. Shin, *Acta Biomater.* **2022**, *149*, 96; b) Z. Yang, H. Qiu, X. Li, P. Gao, N. Huang, *Acta Biomater.* **2018**, *76*, 89.